CRYSTAL GROWTH & DESIGN

Article

Characterization of Pharmaceutical Cocrystals and Salts by Dynamic Nuclear Polarization-Enhanced Solid-State NMR Spectroscopy

Li Zhao, Michael P. Hanrahan, Paroma Chakravarty, Antonio G Dipasquale, Lauren Elizabeth Sirois, Karthik Nagapudi, Joseph W. Lubach, and Aaron J Rossini

Cryst. Growth Des., **Just Accepted Manuscript** • DOI: 10.1021/acs.cgd.8b00203 • Publication Date (Web): 15 Feb 2018

ACS Publications

Crystal Growth & Design is published by the American Chemical Society. 1155 Sixteenth Street N.W., Washington, DC 20036

Characterization of Pharmaceutical Cocrystals and Salts by Dynamic Nuclear Polarization-Enhanced Solid-State NMR Spectroscopy

Li Zhao,[1,2] Michael P. Hanrahan,[1,2] Paroma Chakravarty,[3] Antonio G. DiPasquale,[3] Lauren E. Sirois,[3] Karthik Nagapudi,[3] Joseph W. Lubach,[3]* and Aaron J. Rossini[1,2]**

[1]*Iowa State University, Department of Chemistry, Ames, IA, USA, 50011*

[2]*US DOE Ames Laboratory, Ames, Iowa, USA, 50011*

[3]*Genentech, Inc., Department of Small Molecule Pharmaceutical Sciences, 1 DNA Way, South San Francisco, CA, USA 94080*

AUTHOR INFORMATION

Corresponding Authors

*e-mail: arossini@iastate.edu

*e-mail: lubach.joseph@gene.com

*e-mail: nagapudi.karthik@gene.com

ABSTRACT

Multicomponent solids such as cocrystals have emerged as a way to control and engineer the stability, solubility and manufacturability of solid active pharmaceutical ingredients (APIs). Cocrystals are typically formed by solution- or solid-phase reactions of APIs with suitable cocrystal coformers, which are often weak acids. One key structural question about a given multicomponent solid is whether it should be classified as a salt, where the basic API is protonated by the acid, or as a cocrystal, where the API and coformer remain neutral and engage in hydrogen bonding interactions. It has previously been demonstrated that solid-state NMR spectroscopy is a powerful probe of structure in cocrystals and salts of APIs, however, the poor sensitivity of solid-state NMR spectroscopy usually restricts the types of experiments that can be performed. Here relayed dynamic nuclear polarization (DNP) was applied to reduce solid-state NMR experiments by one to two orders of magnitude for salts and cocrystals of a complex API. The large sensitivity gains from DNP facilitates rapid acquisition of natural isotopic abundance ^{13}C and ^{15}N solid-state NMR spectra. Critically, DNP enables double resonance ^{1}H-^{15}N solid-state NMR experiments such as 2D ^{1}H-^{15}N HETCOR, ^{1}H-^{15}N CP-build up, $^{15}N\{^{1}H\}$ *J*-resolved/attached proton tests, ^{1}H-^{15}N DIPSHIFT and ^{1}H-^{15}N PRESTO. The latter two experiments allow ^{1}H-^{15}N dipolar coupling constants and H-N bond lengths to be accurately measured, providing an unambiguous assignment of nitrogen protonation state and definitive classification of the multicomponent solids as cocrystals or salts. These types of measurements should also be extremely useful in the context of polymorph discrimination, NMR crystallography structure determination and for probing hydrogen bonding in a variety of organic materials.

KEYWORDS Active Pharmaceutical Ingredients, Pharmaceutics, Multicomponent Solids, NMR Crystallography, DNP.

Introduction

Multicomponent solids such as cocrystals have attracted significant interest as a way to control and engineer the stability, solubility and manufacturability of solid active pharmaceutical ingredients (APIs).[1-7] Cocrystals are typically formed by solution phase reaction, melt recrystallization or mechanochemical reaction of APIs with suitable coformers, which are often weak acids.[1-3,5,6] One key problem in the field of pharmaceutical cocrystals is determining whether or not an acid-base reaction between the coformer and API has occurred, resulting in a salt. In a salt the API is protonated by the acid, whereas in a true cocrystal the API and coformer remain neutral and engage in hydrogen bonding and van der Waals interactions within the crystal lattice. We also note that there exists the possibility of a continuum in which the proton in question is shared between the acid and the base along the vector of the hydrogen bond.[8] Temperature may also affect the location of hydrogen bonded protons.[9,10]

Whenever possible, the solid-state structure and hydrogen atom positions in multicomponent solids are usually determined by using single crystal X-ray diffraction, or in some cases neutron diffraction. However, multicomponent solids that are synthesized by mechanochemical methods (a common method of cocrystal screening)[11] usually result in fine powders, making it difficult or impossible to obtain diffraction quality single crystals. Furthermore, even when diffraction quality crystals can be obtained, locating hydrogen atoms is a challenge for single crystal X-ray diffraction.[12,13] For these reasons alternative techniques such as infrared (IR),[3,14] X-ray photoelectron (XPS)[15,16] and solid-state nuclear magnetic resonance (NMR) spectroscopies have been applied to differentiate cocrystals and salts.[17] Of these spectroscopic techniques, only solid-state NMR has the potential to selectively and quantitatively determine location and bond lengths in salt/cocrystal systems.

Solid-state NMR spectroscopy is a powerful probe of molecular structure for cocrystals, salts and pure APIs.[8,18-21] With regards to discriminating between salts and cocrystals, isotropic ^{15}N chemical shifts are very sensitive to the local environment of the nitrogen atoms and protonation usually induces a substantial shift to lower frequency as compared to the API free base, particularly for heterocyclic bases.[22-24] ^{15}N solid-state NMR spectroscopy has been extensively applied to determine the protonation states of the basic nitrogen atoms of APIs within salts, cocrystals and other solid drug forms, such as amorphous solid dispersions.[15,22,23,25-29] Other NMR-active nuclei and more advanced solid-state NMR experiments have also been employed to investigate cocrystals. For example, Brown and co-workers have applied fast magic-angle spinning (MAS) 2D ^{1}H-^{14}N dipolar-heteronuclear multiple-quantum coherence (D-HMQC) experiments to probe the proximity of hydrogen and nitrogen atoms in cocrystals and amorphous dispersions.[30] Brown and co-workers also showed that solid-state ^{1}H-^{15}N scalar attached proton tests (APT)/*J*-resolved experiments[31] could be used to definitively determine if a particular nitrogen was protonated and hence differentiate salts from cocrystals.[25] Very recently Desiraju and co-workers have applied proton detected, fast MAS, cross-polarization (CP) variable contact time (CP-VC) experiments to measure ^{1}H-^{15}N dipolar couplings and inter-atomic distances in simple salts and cocrystals with natural isotopic abundance of ^{15}N.[8] ^{1}H and ^{13}C chemical shifts, 2D ^{1}H-^{1}H homonuclear correlation and 2D ^{1}H-^{13}C heteronuclear correlation (HETCOR) experiments have also proven useful to locate hydrogen atom positions and probe interactions between APIs and coformers.[20,26,32-34] Brunklaus and co-workers have used ^{1}H and ^{13}C solid-state NMR experiments in combination with DFT calculations and powder X-ray diffraction (P-XRD) to solve the crystal structures of multicomponent solids.[33,35] A variety of

^{15}N solid-state NMR experiments have also been applied to understand nitrogen protonation states in organic solids and materials[36-41] and biological systems.[24,42,43]

Unfortunately, the sensitivity of solid-state NMR spectroscopy is intrinsically poor and many of the aforementioned experiments require extremely long experiment times when samples have ^{15}N at natural isotopic abundance [NA(^{15}N) = 0.37%]. For example, 1D ^{15}N solid-state NMR experiments on natural abundance samples typically require many hours or even days of signal averaging obtain spectra with adequate signal-to-noise ratio (SNR).[22] Previous ^{1}H-^{15}N scalar APT/*J*-resolved experiments on a cocrystal required more than 4 days of experiment time.[25] Measurement of ^{1}H-^{15}N dipolar couplings with CP-VC experiments required 3 to 5 days per sample, even though fast MAS and proton detection were employed to boost sensitivity.[8] Schnell and Saalwachter applied proton detected ^{1}H-^{15}N transferred echo double resonance (TEDOR) experiments to measure N-H bond lengths in histidine•HCl•H_2O, although, total experiment times were not provided.[41]

High field dynamic nuclear polarization (DNP) has recently emerged as a method to enhance the sensitivity of solid-state NMR by several orders of magnitude.[44-47] In a modern DNP experiment the high spin polarization of unpaired electrons are transferred to NMR active nuclei, typically ^{1}H.[44-47] DNP can be used to hyperpolarize the ^{1}H nuclei in the interior of powdered microcrystalline solids, such as APIs, in an approach known as relayed DNP.[48-52] Typically, powdered organic solids are prepared for a relayed DNP experiment by grinding them to reduce particle size, then impregnating[53] the powders with a suitable liquid containing a dissolved radical polarizing agent.[49,52] The liquid used for the impregnation step must also be a non-solvent for the solid material and should also be compatible with DNP.[54] During a relayed DNP experiment, DNP-enhanced ^{1}H polarization builds up at the surface of the impregnated particles

and is then transported into the interior of the particles by ^{1}H spin diffusion.[48-50,52] Sensitivity gains of up to two orders of magnitude have been obtained for organic solids, including APIs, with the relayed DNP approach.[48-52] This has enabled solid-state NMR experiments on microcrystalline solids which were previously considered challenging or impossible. For example, relayed DNP has also been applied to enhance the sensitivity of natural isotopic abundance ^{13}C and ^{15}N solid-state NMR experiments on formulated APIs with low drug loading[50] and enabled acquisition of dipolar and scalar ^{13}C-^{13}C homonuclear[49,50,55-58] and ^{13}C-^{15}N heteronuclear 2D correlation NMR spectra.[59] Relayed DNP has also been used to accelerate solid-state NMR experiments with unreceptive isotopes such as ^{2}H,[60] ^{14}N,[61] ^{15}N,[50,61,62] ^{17}O,[63] ^{35}Cl,[64] ^{43}Ca,[65] and ^{89}Y.[66]

Here we apply DNP-enhanced solid-state NMR spectroscopy to the multicomponent solids formed by the co-crystallization of an API (compound **A**) with the counteracid coformers phosphoric acid (**1**), fumaric acid (**2**) and tosylic acid (**3**) (Scheme 1). Comparison of conventional and DNP-enhanced ^{13}C and ^{15}N solid-state NMR spectra of the multicomponent solids **A1**-**A3** illustrates that relayed DNP provides an order of magnitude gain in absolute sensitivity, without any significant reduction in spectral resolution. The large sensitivity gains from DNP facilitate a range of double resonance ^{1}H-^{15}N solid-state NMR experiments including 2D ^{1}H-^{15}N HETCOR, ^{1}H-^{15}N CP-build up, ^{15}N{^{1}H} *J*-resolved/scalar coupling APT, ^{1}H-^{15}N DIPSHIFT and ^{1}H-^{15}N PRESTO. The solid-state ^{15}N{^{1}H} *J*-resolved experiments indicates whether or not each nitrogen atom is protonated and allow the ^{1}H-^{15}N *J*-coupling constant to be estimated. The ^{1}H-^{15}N DIPSHIFT/PRESTO experiments allow the ^{1}H-^{15}N dipolar coupling constants and N-H internuclear distances to be measured, allowing the solids to be unambiguously classified as salts or cocrystals.

Results and Discussion

Description of cocrystals and salts under study. We have applied DNP-enhanced solid-state NMR spectroscopy to study model cocrystals/salts of the pharmaceutical denoted as compound **A** (Scheme 1). **A** was originally under development for treatment of autoimmune diseases including psoriasis and rheumatoid arthritis. Due to a number of undesirable solid-state properties of the free base **A**, including poor stability, solubility, and crystallinity, several cocrystals and salts were screened in attempt to enhance the solubility and other physicochemical characteristics. Multicomponent solids of **A** were obtained through solution- or slurry-based crystallization with the coformers/counteracids phosphoric acid (**1**), fumaric acid (**2**), and tosylic acid (**3**) (Scheme 1), and the resulting solids are denoted as **A1**, **A2** and **A3**, respectively. The crystal structures of **A1**, **A2** and **A3** were determined with single-crystal X-ray diffraction (SC-XRD). The SC-XRD structures illustrate that **A1** and **A3** have a 1:1 stoichiometry of **A** and the respective acid (Figure S1). The crystal structure of **A2** shows that there is a 2:1 stoichiometry of **A** and fumaric acid, consistent with the fact that fumaric acid is a di-carboxylic acid. The multicomponent solids **A1-A3** are an ideal model system to demonstrate the capabilities of DNP-enhanced solid-state NMR for distinguishing cocrystals and salts and determining protonation sites of APIs because SC-XRD structures are available and the acid coformers have a range of acid dissociation constants (pK_a).

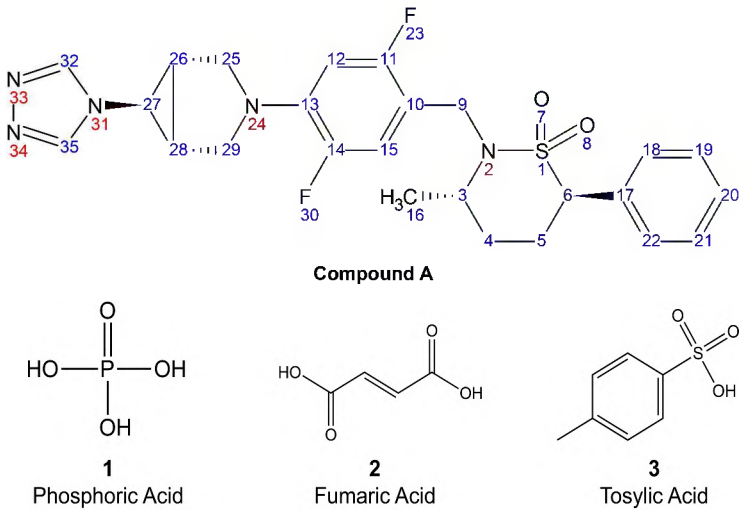

Scheme 1. Molecular structures of the API, compound **A** ((1R,5S,6S)-3-(2,5-difluoro-4-{[(3S,6R)-3-methyl-1,1-dioxido-6-phenyl-1,2-thiazinan-2-yl]methyl}phenyl)-6-(4H-1,2,4-triazol-4-yl)-3-azabicyclo[3.1.0]hexane) and the coformers, phosphoric acid (**1**), fumaric acid (**2**) and tosylic acid (**3**), discussed in this study. The nitrogen atoms of **A** are labelled as N2, N24, N31, N33 and N34.

The classification of **A1**-**A3** as cocrystals or salts can be predicted by considering the pK_a of the API and coformers.[67,68] The SC-XRD structures show that in all of the solids, the N33/N34 nitrogen atoms of **A** will be either protonated or engage in hydrogen bonding interactions with the acidic hydrogen atoms. In order to simplify the discussion, we denote N33 as the nitrogen atom which is in the closest proximity to the acid hydrogen atom, while N34 is non-protonated or the more distant nitrogen atom from the acid hydrogen atom. The most basic pK_a value of compound **A** (conjugate acid) was found to be 2.8 for N33/N34 by fitting the experimental pH-solubility curve to the rearranged Henderson-Hasselbalch equation. The pK_a values for phosphoric acid, fumaric acid and tosylic acid are *ca.* 2.0, 3.0, and –1.3, respectively, for the first acid proton. When the difference in pK_a of the API (the base) and the pK_a of acid [ΔpK_a = pK_a(base) – pK_{a1}(acid)] is greater than 2-3, then the hydrogen atom will usually be transferred from the acid to the base and a salt will result.[67,68] As expected from the ΔpK_a value for **A3** (ΔpK_a = 4.1), the SC-XRD structure indicates that N33 is protonated by inspection of the Fourier

difference map (the N-H bond length is set to 0.88 Å in the SC-XRD structure, *vide infra*).[69] Therefore, **A3** is classified as a salt. Unfortunately, ΔpK_a is often inaccurate or ambiguous for predicting cocrystal/salt formation for the solids when $0 \leq \Delta pK_a \leq 3$.[70] For **A1** (phosphoric acid) $\Delta pK_a = 0.8$ and for **A2** (fumaric acid) $\Delta pK_a = -0.2$. The SC-XRD structures of **A1** and **A2** indicate that all hydrogen atoms remain associated with the acids and are not covalently bonded to N33 or N34 (Figure S1), again through inspection of the Fourier difference map. In addition, the crystal structures of **A1** and **A2** suggest that there is hydrogen bonding between the acidic protons and N33 with N-H distance of *ca.* 1.82-1.84 Å. However, the H atom positions measured by SC-XRD are known to be inaccurate and are usually placed and locations refined using a riding model, where the bond distance to the parent atom is based upon accepted X-H bond distances at the given measurement temperature.[71] Below we describe how DNP-enhanced solid-state NMR spectroscopy can be used to precisely measure N-H bond lengths and quantitatively define hydrogen bonding interactions.

Preparation of samples for DNP-enhanced solid-state NMR spectroscopy. The method used to introduce the exogenous biradical polarizing agents and prepare the samples for DNP experiments has a large impact on both the resolution of the solid-state NMR spectra and the magnitude of the DNP signal enhancement (ε). Microcrystalline organic solids are typically prepared for relayed DNP experiments by grinding the powdered solids to reduce the particle size and maximize DNP enhancements, then impregnating the ground powder with a biradical polarizing agent solution.[49] The liquid used for the impregnation step must be a DNP compatible solvent,[54] however, it must also not dissolve the solid or cause it to transform to another phase.[49,72] It has previously been shown that for some solid forms of theophylline both grinding and impregnation with a solvent can induce phase transitions to other polymorphic forms.[72]

Therefore, the stability of **A3** towards grinding and impregnation was tested by comparing the ^{13}C and ^{15}N solid-state NMR spectra of **A3** impregnated with different solvents, both before and after grinding (see the Supporting Information for a complete description). The tests on **A3** (Figure S2) suggested that samples of **A1**-**A3** should be prepared for DNP experiments by using as-synthesized, unground materials. 1,3-dibromobutane (DBB) was used as the impregnating liquid to prevent transitions to different solid forms. However, we note that 1,3-DBB is not an optimal solvent for DNP experiments because it typically only provides solvent proton DNP enhancements on the order of 50 to 75 with TEKPol as the polarizing agent. In later experiments we instead used mixtures of 1,3-DBB and deuterated 1,4-dibromobutane-d_8 to obtain solvent proton DNP enhancements above 100 (see the Experimental section for a brief discussion). The nitroxide biradical TEKPol[73] was used as the polarizing agent in all experiments.

Comparison of conventional and DNP-enhanced solid-state NMR spectra. The conventional room temperature (293 K) and DNP-enhanced (110 K) ^{13}C and ^{15}N solid-state NMR spectra of **A1**, **A2** and **A3** are compared in Figure 1 and Figure 2, respectively. In all cases cross-polarization magic-angle spinning (CPMAS)[74,75] was used to obtain the solid-state NMR spectra. Conventional room temperature ^{13}C and ^{15}N CPMAS sold-state NMR spectra of **A1**-**A3** were obtained with an 11.7 T (ν_0 = 500 MHz) spectrometer and 4 mm diameter rotors. The DNP-enhanced ^{13}C and ^{15}N solid-state NMR spectra were obtained with 3.2 mm diameter rotors and sample temperatures of *ca.* 110 K. ^{13}C CPMAS DNP enhancements ($\varepsilon_{C\,CP}$) factors ranging from 11 to 23 were measured for **A1**-**A3** by comparing the 110 K CPMAS NMR spectra obtained with and without microwave irradiation (Table S1). In all cases, the $\varepsilon_{C\,CP}$ was estimated to be above 50 for the frozen 1,3-DBB solvent at the surface of the crystal particles. The proton longitudinal

relaxation times ($T_1(^1H)$) of **A1-A3** were measured to be between 10.6 s and 22.5 s at 110 K (Table S1). Long $T_1(^1H)$ (and small particle sizes) are required to obtain high DNP enhancements with relayed DNP.[48,49] However, the relatively moderate $T_1(^1H)$ observed for **A1-A3** also allows optimal recycle delays of ca. 15 to 25 s to be used for NMR experiments.

The sensitivity (S) was also determined for each ^{13}C and ^{15}N solid-state NMR spectrum by measuring the SNR of each spectrum, then dividing it by the square root of the total experiment time (t) in minutes ($S = \text{SNR} \times t^{-1/2}$). Comparison of the sensitivity of the conventional and DNP-enhanced ^{13}C and ^{15}N solid-state NMR spectra for **A1-A3** shows that the gain in absolute sensitivity provided by DNP was between a factor 2-11, which corresponds to a 4- to 121-fold reduction in the total experiment time (Figure 1 and Figure 2). The large gain in sensitivity provided by DNP allows the ^{13}C and ^{15}N solid-state NMR spectra to be obtained in a few minutes while the conventional NMR spectra require hours/days of experiment time to achieve a similar SNR. Importantly, Figure 1 and Figure 2 also illustrate that conventional and DNP-enhanced $^{13}C/^{15}N$ solid-state NMR spectra have very similar resolution. Most of the ^{13}C and ^{15}N isotropic chemical shifts are identical, indicating that no phase transformation was caused by impregnation with 1,3-DBB/TEKPol or by cooling to 110 K. Notably, the ^{13}C NMR signals with the lowest isotropic chemical shifts that are attributed to the methyl group of **A** are either absent or of significantly reduced intensity in the DNP-enhanced ^{13}C NMR spectra. The reduced methyl group ^{13}C NMR signal intensity is likely due to interference between the methyl group rotation and the decoupling/CP spin lock pulses.[76]

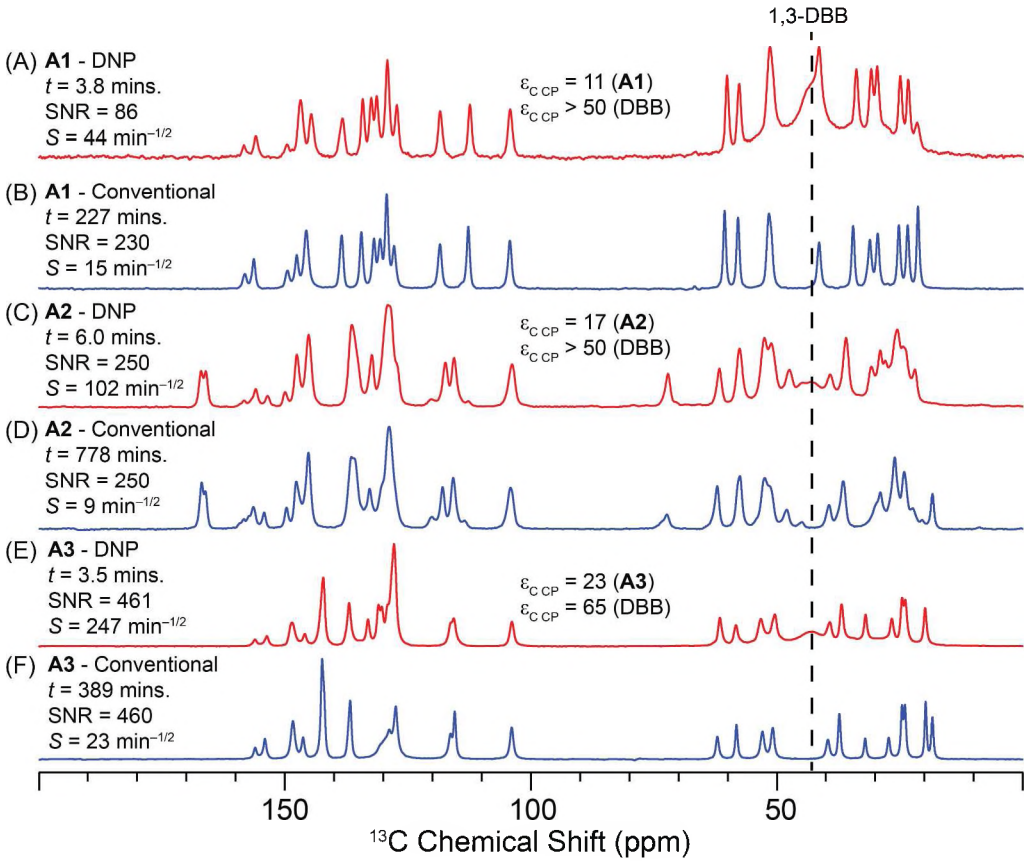

Figure 1. Comparison of DNP-enhanced (upper red traces, 110 K) and conventional (lower blue traces, 293 K) ^{13}C solid-state NMR spectra of cocrystals **A1** (A-B), **A2** (C-D) and **A3** (E-F). The ^{13}C CPMAS DNP enhancements ($\varepsilon_{C\ CP}$) measured for the solvent and the solid phase are indicated. The total experiment time (*t*), signal-to-noise ratio (SNR) and sensitivity (*S*) are indicated for each spectrum. The black dash line indicates the position of DNP solvent 1,3-DBB. All ^{13}C CPMAS NMR spectra were acquired with total sideband suppression (TOSS).[77,78]

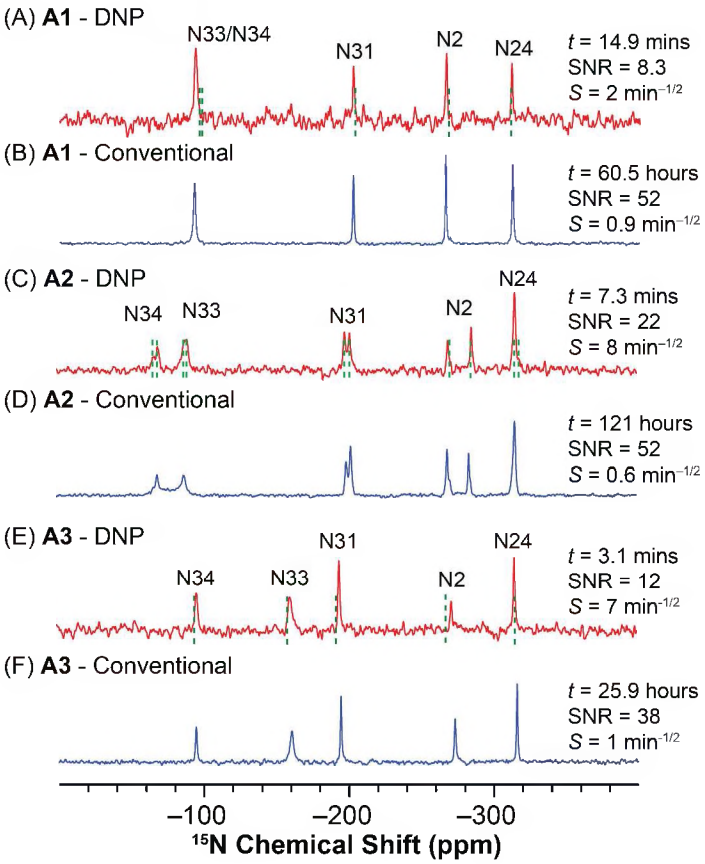

Figure 2. Comparison of DNP-enhanced (upper red traces, 110 K) and conventional (lower blue traces, 293 K) ^{15}N CPMAS solid-state NMR spectra of **A1**, **A2** and **A3**. The total experimental times (*t*), signal-to-noise ratio (SNR) and sensitivity (*S*) are indicated for each spectrum. Isotropic ^{15}N chemical shifts predicted by plane-wave DFT calculations are shown as dashed green lines overlaid on the DNP-enhanced ^{15}N CPMAS NMR spectra.

Distinguishing salts and cocrystals with ^{15}N solid-state NMR. The ^{15}N solid-state NMR spectra can be used to confirm assignment of **A1** and **A2** as cocrystals and **A3** as a salt. First, the isotropic ^{15}N chemical shifts were assigned based upon previously established chemical shift trends.[79] For **A1**-**A3** the ^{15}N NMR signals with chemical shifts between *ca.* –70 ppm to –94 ppm are assigned to the pyrazole nitrogen atoms (N33/N34). The ^{15}N NMR signals at –195 ppm, –270 ppm and –315 ppm are assigned to N31, N2 and N24, respectively. Experimental isotropic ^{15}N chemical shifts were also compared to those obtained from plane-wave DFT calculations for all three samples (Figure 2 and Table S2, see below). In all cases there is excellent agreement

between experimental and calculated ^{15}N isotropic chemical shift values, confirming the ^{15}N peak assignments.

Comparison of the ^{15}N CPMAS NMR spectra of **A1**-**A3** show that the N33 resonance is shifted to a much more negative chemical shift of –161 ppm in **A3**, as compared to the observed chemical shifts of –93 ppm and –88.8/-90.6 ppm for N33 in **A1** and **A2**, respectively. N34 remains much less shielded at –95 ppm in **A3**. Protonation of a nitrogen atom usually induces a more negative ^{15}N chemical shift (the ^{15}N nucleus becomes more shielded) in comparison to the free base.[22,25] Therefore, the ^{15}N chemical shift of N33 within **A3** strongly suggests that the tosylic acid hydrogen atom has been transferred to N33, consistent with the SC-XRD structure of **A3** (*vide supra*). However, in general the observation of a change in the isotropic ^{15}N chemical shift does not imply with certainty that a particular nitrogen site has been protonated because mechanisms other than protonation may also cause changes in the nitrogen chemical shifts. For example, the ^{15}N chemical shifts of the N33 atoms in **A2** have a more positive chemical shift than any of the N33 or N34 ^{15}N NMR signals in **A1** or **A3**, despite the fact that both DIPSHIFT and DFT calculations indicate that N33 is hydrogen bonded to the fumaric acid protons in **A2** (*vide infra*). Furthermore, the use of ^{15}N isotropic chemical shift comparisons to determine protonation sites requires that the chemical shift of the free base can also be measured or calculated. In this case pure **A** was amorphous and it was difficult to obtain ^{15}N solid-state NMR spectra. However, **A1** and **A2** could be used as reference samples to determine that the ^{15}N chemical shift of N33 is more negatively shifted in **A3**. With the high sensitivity enhancements provided by DNP it is possible to perform more advanced ^{15}N solid-state NMR experiments such as variable contact time ^{1}H-^{15}N CPMAS, 2D ^{1}H-^{15}N HETCOR, ^{15}N{^{1}H} solid-state J-

resolved/attached proton tests (APT), ^{1}H-^{15}N DIPSHIFT and ^{1}H-^{15}N PRESTO experiments that provide a definitive assessment of the N-H internuclear distances.

^{1}H-^{15}N Variable Contact Time CPMAS Experiments. One of the simplest solid-state NMR experiments to determine if a particular nitrogen atom is bonded to hydrogen is to acquire ^{1}H-^{15}N CPMAS spectra with different CP contact times.[22] Recently, Desiraju and co-workers have applied fast MAS ^{1}H-^{15}N CP-VC experiments to directly measure ^{1}H-^{15}N dipolar couplings (b_{NH}) and the corresponding internuclear distances (r_{NH}).[8] In a ^{1}H-^{15}N CPMAS experiment the CP signal build-up time constant (T_{NH}) is inversely proportional to the magnitude of the ^{1}H-^{15}N dipolar coupling constant (b_{NH}). The dipolar coupling constant is inversely proportional to the cube of the N-H internuclear distance ($b_{NH} \propto r_{NH}^{-3}$).

Figure S3 shows the ^{1}H-^{15}N CPMAS spectra of **A1**-**A3** acquired with short (less than 500 μs) and long (5 ms) CP contact times. Typically only signals from protonated nitrogen atoms will be observed with short contact times.[22] The CP signal of N33 (–161 ppm) in **A3** is clearly visible in the short contact time spectrum (588 μs), while in all other samples there is little observable signal at short contact times, confirming that N33 in **A3** is indeed protonated. Note that with fast MAS it is possible to directly determine the ^{1}H-^{15}N dipolar coupling constant by observing dipolar oscillations of the ^{1}H-^{15}N CPMAS NMR signal with variable CP contact times.[8] However, the DNP NMR experiments here were performed with relatively slow MAS frequencies, consequently, the dipolar oscillation of ^{1}H-^{15}N CP signal intensity will be damped by ^{1}H spin diffusion. DNP-enhanced ^{1}H-^{15}N CPMAS NMR spectra of **A1**-**A3** obtained with variable CP contact time were fit to determine the CP build-up time constant (T_{NH}, Figure S3) and qualitatively probe the H-N dipolar couplings and bond lengths. For the protonated N33 in **A3**, T_{NH} = 0.6 ± 0.1 ms, which corresponds to the smallest T_{NH} (fastest CP build-up rate). As

expected all other nitrogen atoms in **A1**-**A3** show significantly larger T_{NH} between 1.4-2.8 ms (Figure S3), consistent with a lack of covalently attached protons for these sites and the corresponding slow CP build-up rates.

2D ^{1}H-^{15}N CP-HETCOR Experiments. 2D ^{1}H-^{15}N CP-HETCOR spectra obtained with short contact times provide correlations between dipolar coupled ^{1}H and ^{15}N spins which allows their proximity to be directly confirmed. The 2D CP-HETCOR spectra also provide access to high resolution ^{1}H solid-state NMR spectra because ^{1}H homonuclear dipolar decoupling is applied during the indirect dimension evolution period (t_1). Here, e-DUMBO$_{1\text{-}22}$ homonuclear decoupling[80] was applied. The DNP-enhanced 2D ^{1}H-^{15}N CP-HETCOR spectra of **A1**-**A3** were obtained in less than 4 hours total experiment time each (Figure 3). 2D ^{1}H-^{13}C CP-HETCOR spectra of **A1**-**A3** were also obtained with experiment times less than 1 hour each (Figure S4). The 2D ^{1}H-^{15}N and ^{1}H-^{13}C CP-HETCOR spectra allow all of the ^{1}H chemical shifts to be measured with high resolution. ^{1}H chemical shifts are potentially useful constraints for DFT-driven NMR crystallography structure determination or refinement.[81-87]

Figure 3A shows the ^{1}H-^{15}N CP HETCOR spectrum of **A3** which was obtained in only 3.3 h with a relatively short CP contact time (τ_{CP}) of 320 μs. The short contact time results in a selective polarization transfer from the acid hydrogen with a chemical shift of *ca.* 16.8 ppm to the protonated N33 nitrogen (δ_{iso} = –161 ppm). This correlation is consistent with a large b_{NH}, which implies that the acid hydrogen atom is directly bonded to N33 in **A3**. A ^{1}H-^{15}N CP-HETCOR spectrum of **A3** was also obtained with τ_{CP} = 2 ms (Figure 3B). This HETCOR spectrum also shows an intense correlation between the acid proton ^{1}H NMR signal and the N33 ^{15}N NMR signal again. The 2 ms contact time CP-HETCOR spectrum also shows additional correlations between the N33/N34 ^{15}N NMR signals and aromatic/alkene ^{1}H NMR signals

(Figure 3B). These correlations could occur due to long-range dipolar coupling between ^{15}N and the aromatic protons of tosylic acid and/or to the alkene hydrogen atoms attached to C32/C33. However, ^{1}H spin diffusion during the CP contact pulse will lead to relayed correlations in the 2D HETCOR spectra obtained with long contact times, therefore, caution is warranted when trying to assess proximities based upon observation of correlations in the HETCOR spectrum. If required, relayed correlations could be suppressed by using Lee-Goldberg (LG) CP-HETCOR experiments.[88]

The 2D ^{1}H-^{15}N CP-HETCOR spectra of **A1** and **A2** were obtained with τ_{CP} = 2 ms and τ_{CP} = 5 ms, respectively, because all nitrogen sites exhibit slow CP build-up rates (*vide supra*). The 2D ^{1}H-^{15}N CP-HETCOR spectra of **A1** and **A2** show that the N33 signals give rise to weak or negligible correlations to the acid protons of phosphoric and fumaric acid at 14 ppm (Figure 3 and Figure S5) and 17 ppm (Figure 3C), respectively. These weak correlations are consistent with relatively large N-H internuclear distances and correspondingly small b_{NH}. Indeed, the solid-state NMR measurements of b_{NH} and r_{NH} suggest that the H-N33 internuclear distance within **A1** and **A2** are on the order of 1.4 Å to 1.6 Å (*vide infra*).

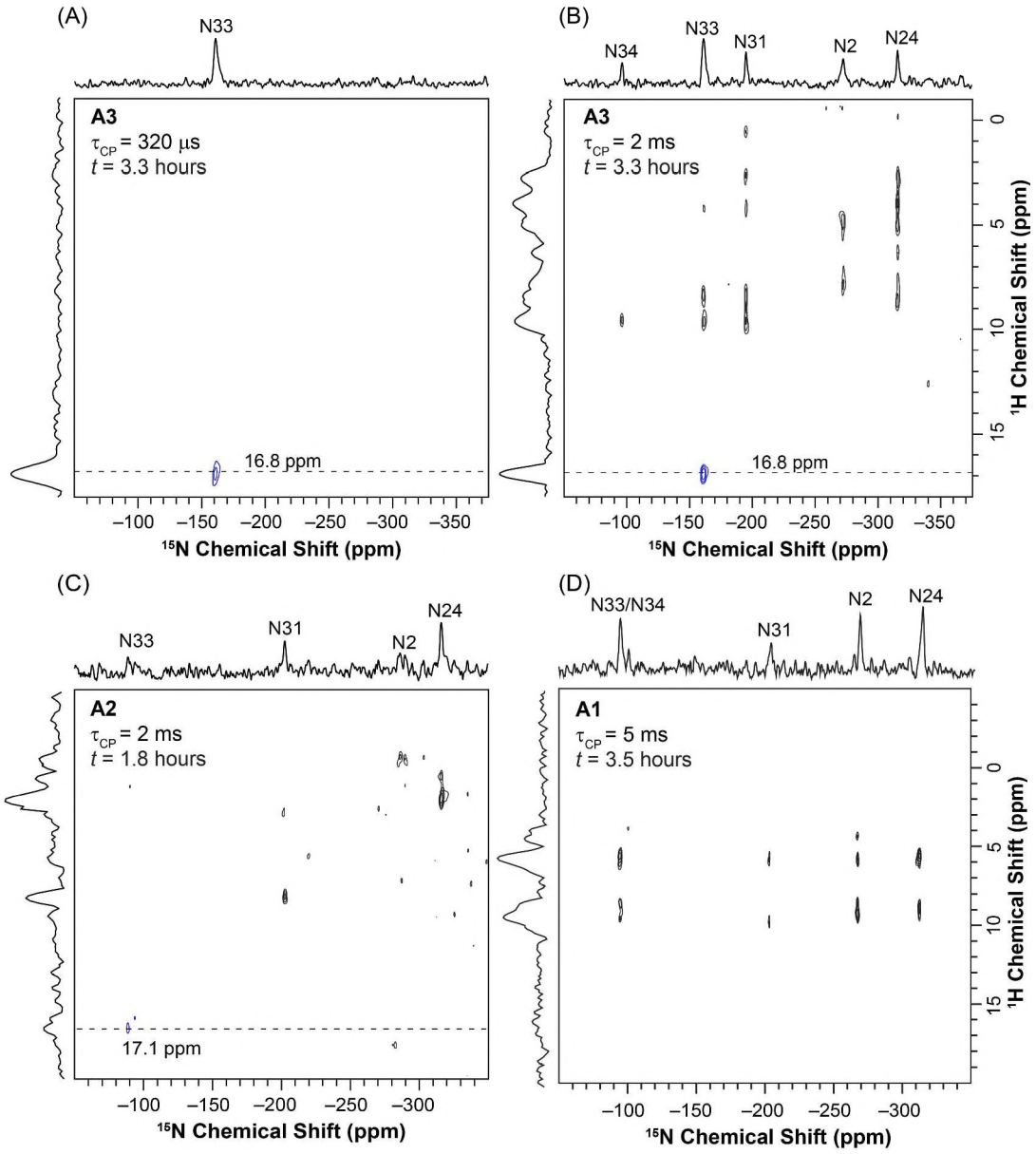

Figure 3. Natural-abundance, DNP-enhanced 2D ^{1}H-^{15}N CP-HETCOR NMR spectra of **A3** acquired with (A) τ_{CP} = 320 μs and (B) τ_{CP} = 2.0 ms in order to probe short and long range N-H distances. 2D HETCOR spectra of (C) **A2** and (D) **A1** were acquired with τ_{CP} = 2.0 ms and 5.0 ms, respectively. Correlations between the acid proton(s) and nitrogen N33 are indicated with blue contours and dashed lines. All spectra were acquired with eDUMBO$_{1\text{-}22}$ ^{1}H homonuclear decoupling scheme applied during the t_1 evolution period with a ^{1}H RF field of ca. 100 kHz. The MAS frequency was 9375 Hz in all cases. Each 2D spectrum was obtained in a total experiment times of 1.8 to 3.5 hours.

$^{15}N\{^{1}H\}$ J-Resolved Experiments. Brown and co-workers previously applied $^{15}N\{^{1}H\}$ *J*-resolved/attached proton test experiments to probe nitrogen protonation in cocrystals/salts of APIs, however, *ca.* 6 days of spectrometer time were required.[25] Here, with the signal enhancement provided by DNP it was possible to perform $^{15}N\{^{1}H\}$ *J*-resolved experiments on **A3** in less than 4 h.

In the $^{15}N\{^{1}H\}$ *J*-resolved solid-state NMR experiments a ^{15}N spin echo NMR spectrum is obtained with ^{1}H homonuclear decoupling applied during the echo delay period to allow evolution of scaled heteronuclear *J*-couplings (Figure S6).[31,89] Application of a ^{1}H π pulse at the center of the spin echo causes evolution of $^{15}N\{^{1}H\}$ *J*-couplings and the attenuation/oscillation of ^{15}N NMR signals which are chemically bonded (scalar coupled) to ^{1}H. Here two sets of ^{15}N NMR spectra were obtained for each *J*-evolution time.[90] A $^{15}N\{^{1}H\}$ *J*-dephased spectrum was obtained with application of simultaneous ^{1}H and ^{15}N π pulses at the center of the spin echo, while the control spectrum was obtained with application of only the ^{15}N π pulse.[90] This allows a normalized *J*-resolved data set to be created where the decay of the ^{15}N NMR signal due to ^{1}H-^{15}N *J*-couplings should not be affected by ^{15}N transverse relaxation.[90]

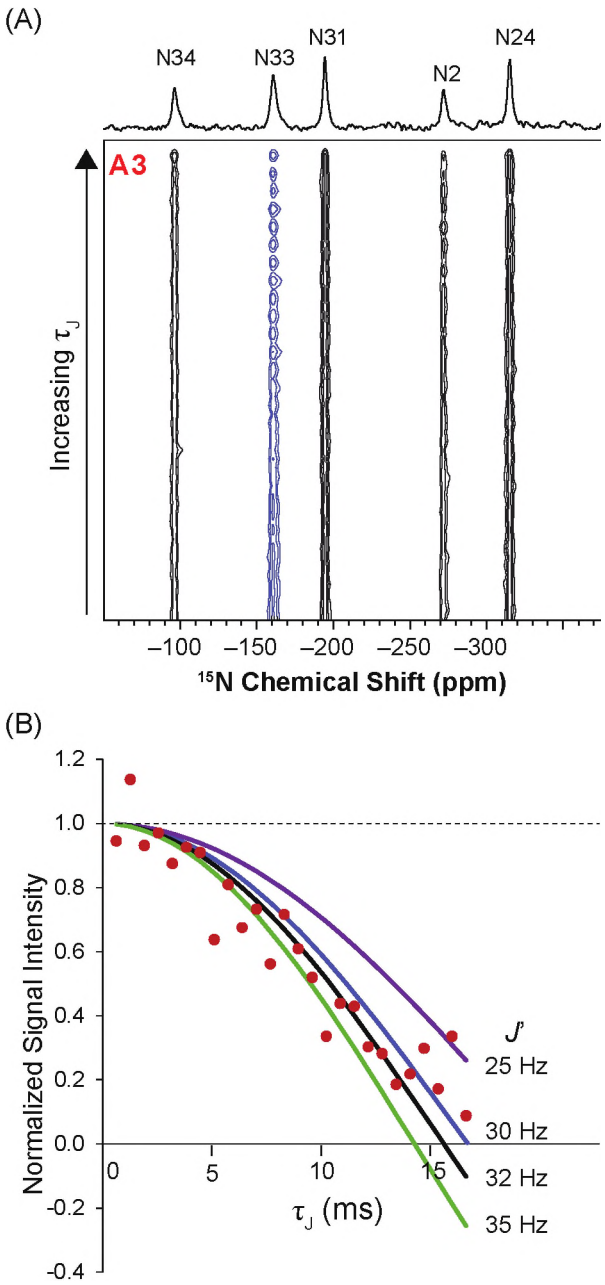

Figure 4. (A) DNP-enhanced $^{15}N\{^1H\}$ *J*-resolved NMR experiment on **A3**. The control and *J*-dephased points are interleaved, resulting in alternating points of high and low intensity for N33. (B) Plot of the experimental, normalized $^{15}N\{^1H\}$ *J*-dephasing curve for the protonated nitrogen, N33 (red circles). The normalized *J*-resolved signal was obtained by dividing the measured intensity of each *J*-dephased point by the intensity of the corresponding control point. The solid lines were calculated with the function *Normalized Signal Intensity* = $\cos(\pi J'_{NH}\tau_J)$. The black curve was calculated with $^1J'_{NH}$ = 32 Hz and $^1J_{NH}$ = 56 Hz and gave the lowest RMSD fit of the experimental data points. For comparison, *J*-dephasing curves are also shown for several other values of $^1J'_{NH}$.

Figure 4A shows the results of the $^{15}N\{^{1}H\}$ *J*-resolved experiment on **A3**. The peak at −161 ppm assigned to the protonated nitrogen N33 is the only site to show a significant reduction in normalized signal intensity with increasing *J*-evolution time (τ_J, defined in Figure S6). Significant *J*-dephasing was not observed for any of the nitrogen NMR signals in **A1** and **A2** (Figure S7). All of the $^{15}N\{^{1}H\}$ *J*-resolved experiment results are consistent with the variable contact time CPMAS and CP-HETCOR experiments which suggested that both **A1** and **A2** are cocrystals and that **A3** is a salt.

For **A3** the normalized *J*-resolved curve was fit to a simple cosine function to estimate the magnitude of the one bond ^{15}N-^{1}H J-coupling ($^{1}J_{NH}$):

$$Normalized\ Signal\ Intensity = \cos\left(\pi\tau_J J'_{NH}\right) \quad (1)$$

where τ_J is the *J*-evolution time and J'_{NH} is the $^{15}N\{^{1}H\}$ *J*-coupling constant scaled by the homonuclear decoupling scaling factor ($J' = s \times J$). A fit of the normalized *J*-resolved curve yields $^{1}J'_{NH}$ = 32 Hz, which after accounting for the e-DUMBO$_{1\text{-}22}$ scaling factor (*s*) of 0.56 gives $^{1}J_{NH}$ = 56 Hz (Figure 4B). For comparison, a $^{1}J_{NH}$ of 92 Hz is typical of the amide groups in the backbone of proteins[91] and plane-wave DFT calculations predicted a $^{1}J_{NH}$ value of 83 Hz for **A3**.

It has previously been shown that *J*-resolved solid-state NMR experiments can be used to measure ^{1}H-^{13}C *J*-couplings and obtain *J*-multiplets for plastic solids such as adamantane[89] and trimethoxybenzene[92] or for mobile and dilute molecules grafted on surfaces.[93,94] To the best of our knowledge, alanine[80,95] and histidine•HCl•H_2O[92] are the only examples of rigid crystalline solid where *J*-resolved experiments have been applied for the measurement of ^{1}H-^{13}C or ^{1}H-^{15}N *J*-couplings. Emsley and co-workers showed that the ^{13}C solid-state NMR spectrum of the methine carbon in alanine gives rise to a doublet under application of e-DUMBO$_{1\text{-}22}$

homonuclear decoupling with both moderate (22 kHz) and fast MAS (65 kHz) frequencies.[80,95] However, in alanine the methine hydrogen atom likely has weak homonuclear dipolar couplings with other protons because the only other proximate protons are in a mobile NH_3^+ group. Therefore, alanine likely has favorable properties that allow for observation of *J*-multiplets under homonuclear decoupling. Pruski and co-workers observed clean doublets in the ^{15}N solid-state NMR spectrum of histidine•HCl•H_2O obtained under PMLG decoupling with a 40 kHz MAS frequency.[92] Other previous *J*-resolved solid-state NMR experiments on crystalline solids only showed NMR spectra obtained with a few *J*-evolution times;[25,31] complete *J*-resolved curves or *J*-multiplets were not shown.

DNP-enhanced $^{13}C\{^1H\}$ *J*-resolved solid-state NMR experiments were performed on histidine•HCl•H_2O to test if solid-state *J*-resolved NMR experiments can accurately measure $^1J_{CH}$ (Figure S8). The normalized $^{13}C\{^1H\}$ *J*-resolved curves showed substantial deviations away from the ideal cosine functions and there is generally poor agreement with $^1J_{CH}$ measured with solution NMR. Room temperature $^{13}C\{^1H\}$ *J*-resolved solid-state NMR experiments performed on histidine•HCl•H_2O with fast MAS frequencies 50 kHz also showed distorted *J*-resolved curves (data not shown). The deviations of the normalized *J*-resolved curves could occur due to incomplete suppression of ^1H spin diffusion by the homonuclear decoupling, RF inhomogeneity, imperfect magic angle setting and evolution of residual heteronuclear dipolar couplings. Therefore, we caution that the $^1J_{NH}$ of 56 Hz measured for **A3** should be treated as an estimate, rather than an accurate measurement of $^1J_{NH}$. Nevertheless, the *J*-resolved experiment unambiguously confirms that the N33 atom in **A3** is covalently bonded to a proton and therefore, **A3** should be classified as a salt.

N-H Dipolar Coupling Measurements and Bond Length Determination. In order to definitively determine protonation states the ^{15}N-^{1}H dipolar coupling constants (b_{NH}) and corresponding N-H internuclear distances (r_{NH}) in **A1**-**A3** were directly measured with constant time dipolar doubled DIPSHIFT[96] and PRESTO-II[97] experiments (see Figure S6 for pulse sequence diagrams). DNP-enhanced ^{13}C-^{1}H/^{15}N-^{1}H DIPSHIFT and PRESTO-II experiments were initially tested on histidine•HCl•H_2O (Figure S9). For histidine•HCl•H_2O the C-H and N-H internuclear distances (r_{CH} and r_{NH}, respectively) measured with both PRESTO-II and DIPSHIFT showed good agreement with those determined using plane-wave DFT calculations and those observed in the single-crystal neutron diffraction structure (Table S3).[98]

Hong and co-workers have previously applied ^{15}N-^{1}H DIPSHIFT experiments to determine the protonation states of ^{15}N-labeled histidine re-crystallized from solutions with different pH.[42] In the dipole-doubled DIPSHIFT experiment two ^{15}N π pulses are applied at different fractions of two rotor periods in order to interfere with MAS and reintroduce heteronuclear dipolar couplings.[96] Frequency-switched LG (FSLG)[99-101] ^{1}H homonuclear decoupling is applied to eliminate ^{1}H spin diffusion during the first rotor period, while the ^{15}N π pulses interfere with the averaging of heteronuclear dipolar couplings by MAS. The ^{15}N-^{1}H DIPSHIFT experiments were performed at a relatively slow MAS frequency (ν_r = 3846 Hz) to allow small b_{NH} couplings to be measured.

The results of ^{15}N-^{1}H DIPSHIFT experiments on samples **A1**-**A3** for the N33 nitrogen atoms that are either covalently bonded or hydrogen bonded to the acid protons are shown in Figure 5A and Figure S10. The $b_{N33\text{-}H}$ and $r_{N33\text{-}H}$ determined from the ^{15}N-^{1}H DIPSHIFT experiments are reported in Table 1. As expected, **A3** was determined to have the largest $b_{N33\text{-}H}$ of 11.8 kHz, corresponding to a N33-H internuclear distance of 1.01 Å. This is consistent with

the SC-XRD structure, plane-wave DFT calculations and all of the other NMR experiments which indicated that the N33 nitrogen atom is protonated in **A3**, and this phase should be considered a true salt. For **A2** and **A1** $r_{N33\text{-}H}$ of 1.43 Å and 1.55 Å, respectively, were determined from the DIPSHIFT curves. The mesaured internuclear distances are consistent with hydrogen bonding interactions between N33 and the acid protons and confirm assignment of **A2** and **A1** as cocrystals.

The PRESTO-II pulse sequence was also applied to measure $b_{N33\text{-}H}$ and $r_{N33\text{-}H}$ in **A3** (Figure 5B). The PRESTO experiment was originally described by Levitt and co-workers.[97] In a PRESTO experiment, symmetry based recoupling pulse sequences are applied to the ^{1}H nuclei to simultaneously decouple ^{1}H homonuclear dipolar couplings and recouple heteronuclear dipolar couplings to enable ^{1}H→X coherence transfer. Variation of the recoupling time in a PRESTO experiment causes an oscillation of the NMR signal. The PRESTO signal oscillation can be simulated to determine the heteronuclear dipolar coupling constant.[97] Recently, Perras and co-workers have recently applied DNP-enhanced PRESTO NMR experiments to measure ^{17}O-^{1}H dipolar coupling constants and corresponding O-H internuclear distances in inorganic solids.[102] For **A3**, comparison of the experimental ^{15}N-^{1}H PRESTO dipolar oscillation to numerical SIMPSON simulations yields $b_{N33\text{-}H}$ = 13.3 kHz. This dipolar coupling constant corresponds to $r_{N33\text{-}H}$ = 0.97 Å and is in reasonable agreement with $r_{N33\text{-}H}$ = 1.01 Å determined with DIPSHIFT (Figure 5A and Figure S10). Below, we compare the $r_{N33\text{-}H}$ measured using ^{1}H-^{15}N double resonance NMR experiments to those determined with optimization of the H-atom positions by plane-wave DFT calculations.

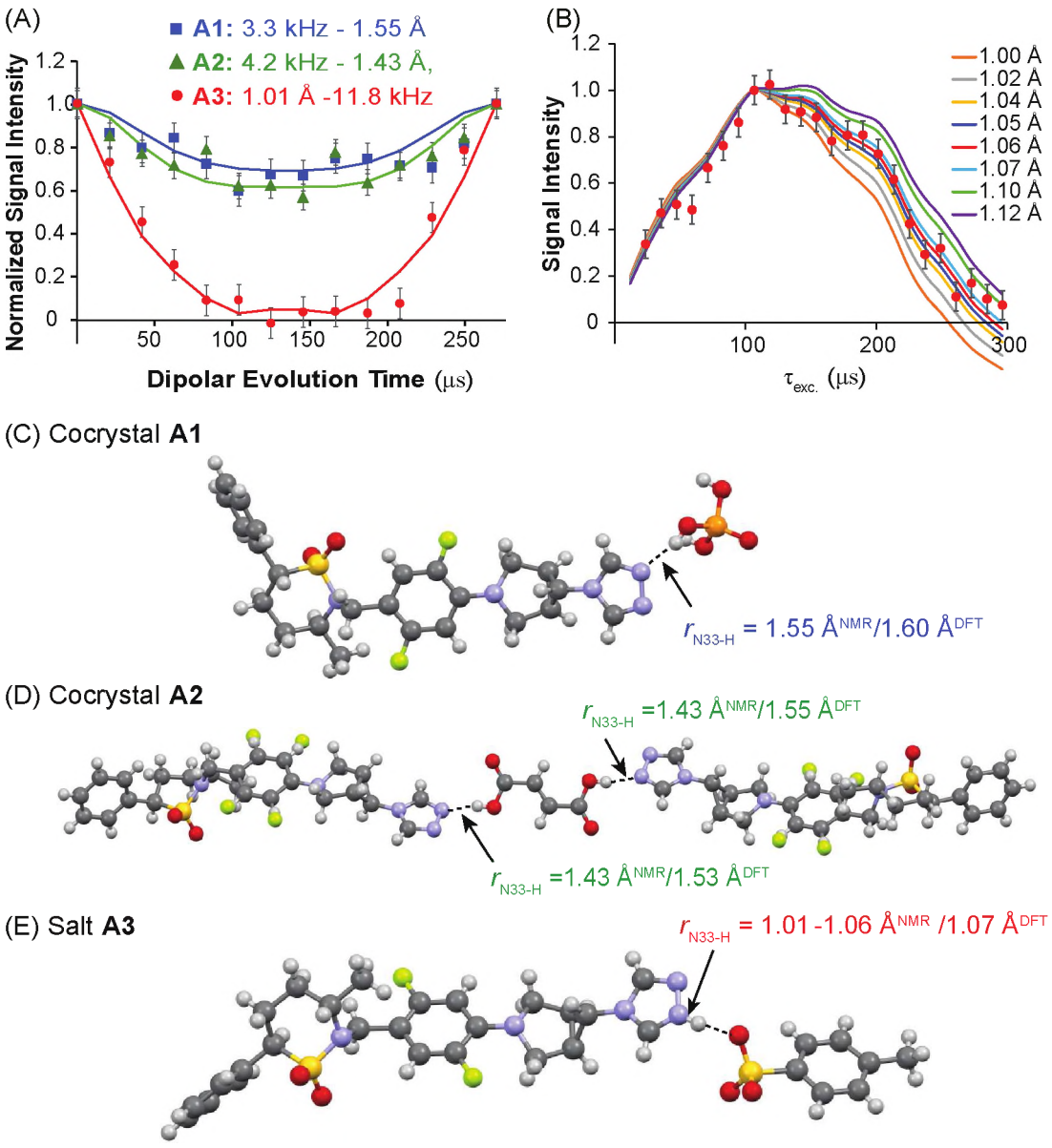

Figure 5. (A) ^{15}N-^{1}H DIPSHIFT dipolar dephasing curves for the N33 nitrogen atoms that are nearest to protons in **A1**-**A3** (solid points). Numerical SIMPSON simulations of DIPSHIFT curves are shown as solid lines and the dipolar coupling constants (b_{NH}) and corresponding N-H distances (r_{NH}) are indicated. (B) Oscillation of the ^{1}H-^{15}N PRESTO solid-state NMR signal of N33 in **A3** (red dots) as a function of the excitation recoupling time (τ_{exc}). Numerical SIMPSON simulations of the PRESTO dipolar oscillations are shown as colored lines for different b_{NH} and $r_{N33\text{-}H}$. Molecular structure of (C) cocrystal **A1**, (D) cocrystal **A2** and (E) salt **A3** with proton positions from geometry optimization with plane-wave DFT calculations. Select $r_{N33\text{-}H}$ are indicated.

Comparison of N-H bond lengths determined with NMR experiments and plane-wave DFT calculations. Plane-wave DFT calculations have been widely applied to optimize the

hydrogen atom positions of X-ray diffraction structures.[13,19,103] The unit cell parameters and heavy atom positions determined from the SC-XRD structures of compounds **A1** – **A3** were fixed and plane-wave DFT was then applied to optimize the proton positions. The DFT optimized $r_{N33\text{-}H}$ were 1.07 Å for **A3**, 1.55 Å / 1.53 Å for **A2** and 1.60 Å for **A1** and these values are in reasonable agreement with $r_{N33\text{-}H}$ determined from the ^{15}N-^{1}H DIPSHIFT solid-state NMR experiments (Table 1). The largest difference between the calculations and experiments is for **A2** which gave a 0.12 Å difference in the $r_{N33\text{-}H}$ determined by DIPSHIFT experiments and the calculations, with the DIPSHIFT experiments suggesting that the bond length is shorter. We note that Steiner and co-workers have shown that sample temperature can cause large variations of up to 0.1 Å in hydrogen bond lengths over the temperature range of 20 – 200 K.[9] Therefore, the temperature used for the NMR experiments could possibly cause substantial variations in the experimentally determined internuclear distances which may explain some of the discrepancies.

Table 1. N33-H Dipolar Coupling Constants (b_{NH}) and N33-H Internuclear Distances ($r_{N33\text{-}H}$) Obtained from Solid-state NMR Experiments and Plane-wave DFT Calculations.

	Experiment - DIPSHIFT		Calculated - Plane-wave DFT	
Sample	b_{NH} (kHz)	$r_{N33\text{-}H}$ (Å)	b_{NH} (kHz)	$r_{N33\text{-}H}$ (Å)
A1	3.3 ± 0.21	1.55 ± 0.1	2.97	1.60
A2	4.2 ± 0.29	1.43 ± 0.1	3.27/3.40[a]	1.55/1.53[a]
A3	11.8 ± 0.35	1.01 ± 0.03	9.94	1.07

[a]Note that **A2** has two inequivalent molecules of **A** within the unit cell (Z' = 2), however, the ^{15}N NMR signals of the two inequivalent N33 sites are not well resolved. Therefore, it is only possible to measure a single distance experimentally.

Conclusions

Here we have shown that relayed DNP enables advanced ^{13}C and ^{15}N solid-state NMR experiments on multicomponent solids consisting of a complex API and organic or inorganic acid coformers. For the solids studied here, relayed DNP provided an absolute gain in sensitivity of factors of ca. 2 to 11 in comparison to conventional solid-state NMR spectroscopy, without any substantial reduction in resolution of the NMR spectra. The gain in sensitivity provided by DNP, corresponding to 4- to 121-fold reduction in experiment times, enables advanced ^{1}H-^{15}N double resonance solid-state NMR experiments that allow H-N internuclear distances to be measured, allowing the solids to be unambiguously classified as salts or cocrystals. The DNP-enhanced solid-state NMR measurements are complementary to SC-XRD and allow the N-H internuclear distances to be experimentally determined. Reasonable agreement was also observed between the experimentally determined N-H internuclear distances and those predicted with plane-wave DFT calculations.

The DNP-enhanced ^{1}H-^{15}N double resonance solid-state NMR experiments applied here should also prove useful in the context of polymorph discrimination and NMR crystallography structure determination. We anticipate that with the large sensitivity gains provided by DNP it should also be possible to perform these types of experiments on pharmaceutical formulations with low API loadings.[50]

EXPERIMENTAL

Synthesis of Multicomponent Solids A1-A3. Compound **A** was synthesized by Genentech for use in pharmaceutical development. **A1** (phosphoric acid cocrystal) was prepared via slurry conversion by first suspending 500 mg of **A** free base in 4 mL of ethyl acetate (EtOAc) at 25 °C, then adding 4 mL of 0.25 M phosphoric acid in EtOAc. The resulting suspension was heated to 50 °C and stirred for 72 h, then cooled to 5 °C and aged for 6 h before vacuum filtration to isolate the solids. The solids were dried under vacuum at 50 °C to yield **A1**. **A2** (hemifumaric acid cocrystal) was prepared from solution by dissolving 500 mg **A** free base in 5 mL acetone at 50 °C, then adding 1 molar equivalent of fumaric acid while stirring. Once crystals began to precipitate the suspension was aged an additional 30 min at 50 °C before cooling to 25 °C over 3 h. Solids were isolated via vacuum filtration, washed with acetone, and dried at 50 °C under vacuum to give **A2**. **A3** was prepared from solution by dissolving 5 g of **A** free base in 50 mL of methyl ethyl ketone (MEK) at 25 °C, then adding 1 molar equivalent of *p*-toluenesulfonic acid monohydrate dissolved in 20 mL MEK. The solution was stirred at 25 °C for 72 h, then allowed to evaporate, yielding the white crystalline solid **A3** (tosylate salt).

Single Crystal X-Ray Diffraction. Details on single crystal X-ray diffraction are provided in the Supporting Information.

Remote DNP sample preparation. 1,3-dibromobutane (1,3-DBB) was used as the impregnating liquid[54] for **A1-A3** because it did not cause phase transitions (see Supporting Information for additional discussion). 1,3-DBB normally provides DNP enhancements on the order of 50 to 75 with the TEKPol polarizing agent. 1,3-DBB likely provides four-fold lower DNP enhancements than 1,1,2,2-tetrachloroethane (TCE) because it has a higher concentration of proton spins (ca. 67 M ^{1}H concentration in DBB vs. 19 M ^{1}H concentration in TCE).

Therefore, a mixture of protonated and deuterated 1,3-DBB could possibly provide higher DNP enhancements by reducing the proton concentration. Unfortunately, deuterated 1,3-DBB was not commercially available, however, fully deuterated 1,4-dibromobutane (1,4-DBB-d_8) was commercially available. In later DNP experiments on cocrystals it was found that using either 50:50 or 25:75 (v:v) mixtures of 1,3-DBB:1,4-DBB-d_8 proton DNP enhancements above 130 could be obtained for the solvent signal. A 50:50 mixture of 1,3-DBB:1,4-DBB-d_8 is recommended as a solvent for DNP experiments in cases where TCE cannot be used. A 16 mM TEKPol TCE solution was used as the impregnating liquid for histidine·HCl·H_2O.

Histidine hydrochloride monohydrate (histidine•HCl•H_2O) and samples **A1-A3** were prepared for DNP experiments by weighing out 30-40 mg of the solids and 6-8 mg of KBr on to a watch glass. Only **A1** and histidine•HCl•H_2O were prepared with a grinding step prior to sample impregnation with the polarizing agent solution. The KBr was added so that ^{79}Br NMR could be used to measure sample temperatures and check the magic angle setting when desired. The powders were then mixed together using a spatula. The powdered mixture was then impregnated with 15-20 μL of the DNP polarizing agent solution (enough to make the sample appear slightly wet). TEKPol was used as the polarizing agent with concentrations of 15 to 20 mM in the radical solution.[73] Once the samples were impregnated they were packed into a sapphire 3.2 mm DNP rotor, with a Teflon screw insert and a zirconia drive cap.

Solid-state NMR Experiments. DNP-enhanced solid-state NMR experiments were performed on a Bruker 9.4 T 400 MHz/263 GHz DNP solid-state NMR spectrometer[104] equipped with a Bruker Avance III console. A Bruker 3.2 mm triple resonance DNP probe, configured in HCN triple resonance mode was used for acquisition of all DNP spectra. The sample temperature for DNP experiments was approximately 110 K. The microwave power for optimal DNP

enhancements was optimized directly on each sample. ^{1}H pulse lengths and RF fields were directly calibrated on the samples of interest. ^{1}H and ^{13}C chemical shifts were referenced with respect to neat tetramethylsilane via an external secondary standard of adamantane. ^{15}N chemical shifts were referenced with respect to nitromethane by using the IUPAC frequency ratio.[105]

All cross-polarization magic angle spinning (CPMAS) experiments[74,106] were performed with a variable amplitude ^{1}H contact pulse which was linearly ramped from 90% to 100% RF field to broaden the Hartmann-Hahn match condition.[107] SPINAL-64 ^{1}H heteronuclear decoupling[108] was applied during signal acquisition with a ^{1}H rf field of ca. 100 kHz. The pulse program used to acquire the 2D ^{1}H-^{13}C and ^{1}H-^{15}N CP-HETCOR spectra is shown in Figure S6.[109] eDUMBO$_{1\text{-}22}$ homonuclear ^{1}H decoupling was applied during the indirect dimension evolution period (t_1) with a ^{1}H RF fields between 100-116 kHz.[80] The MAS frequency for all HETCOR experiments was 9375 Hz. The ^{1}H-^{13}C and ^{1}H-^{15}N HETCOR spectra were typically acquired with 2 to 8 scans per increment, recycle delays of 5 to 23 s, 128 individual t_1 increments, for a total t_1 evolution time of 4.1 ms (for more details see Table S4). The ^{1}H spectral widths were scaled by a factor of 1.8 to correct the scaling of the ^{1}H chemical shift caused by the eDUMBO$_{1\text{-}22}$ homonuclear ^{1}H decoupling.

The pulse sequence for the ^{15}N{^{1}H} *J*-resolved solid-state NMR experiments is shown in Figure S6.[31] For each value of τ_J a ^{15}N{^{1}H} *J*-dephased spectrum was obtained by application of simultaneous ^{1}H and ^{15}N π pulses, while a control spectrum was obtained with application of only the ^{15}N π pulse required to form the ^{15}N spin echo.[90] This results in a normalized *J*-resolved data set where the decay of the ^{15}N NMR signal due to ^{1}H-^{15}N *J*-couplings should not be affected by ^{15}N transverse relaxation. In the *J*-resolved experiments the initial transverse ^{15}N magnetization was generated using CP with a contact time of 5 ms. eDUMBO$_{1\text{-}22}$ decoupling

with an RF field strength between 100-116 kHz and pulse duration of 32 μs was applied to reduce ^{1}H homonuclear spin diffusion during the *J*-coupling evolution period (τ_J). SPINAL-64 heteronuclear decoupling was applied with an RF field of 100 kHz was then applied during acquisition. The MAS frequency for all *J*-resolved experiments was 9375 Hz. The *J*-resolved experiments used recycle delays between 5 to 23 s with 8 to 24 scans acquired per increment and 36-60 total increments. The *J*-evolution time was increased in increments of 640 μs (corresponding to 20 eDUMBO$_{1\text{-}22}$ pulses and 6 rotor cycles).

The pulse sequence used for the PRESTO-II experiment is shown in Figure S6.[97] The PRESTO-II experiments used the symmetry-based R18$_1^7$ dipolar recoupling pulse sequence to achieve ^{1}H→^{13}C/^{15}N coherence transfer via heteronuclear dipolar couplings. The MAS frequency for the PRESTO experiment was 9375 Hz, which corresponds to a 107 μs rotor period. The π pulse width in the R18$_1^7$ recoupling sequence was 5.94 μs (18 π-pulses per rotor period), which corresponds to a 84.375 kHz RF field (18/2 × τ_{rot}). In order to measure ^{1}H-^{15}N dipolar coupling constants with PRESTO-II experiments on histidine•HCl•H$_2$O and **A3** the reconversion period ($\tau_{rec.}$) was fixed to a single rotor cycle, while the duration of the excitation period increased in steps of 11.85 μs (corresponding to a pair of ^{1}H recoupling π-pulses). 100 kHz RF field SPINAL-64 ^{1}H heteronuclear decoupling was applied in all cases. In order to measure ^{1}H-^{13}C dipolar coupling constants with PRESTO-II experiments on histidine•HCl•H$_2$O τ_{rec} was set equal to 71.11 μs (six ^{1}H recoupling π-pulses pairs). This was followed by a delay of 35.56 μs at the start of which the heteronuclear decoupling was turned on and applied for the duration of signal acquisition. The ^{13}C spin echo π-pulse was centered on the rotor cycle. The ^{15}N-^{1}H PRESTO-II experiments on **A3** were acquired with 48 scans for each value of τ_{exc} and a 40 s recycle delay was used (Table S1).

The pulse sequence used for the constant time dipolar doubled DIPSHIFT experiment is shown in Figure S7.[96] The MAS frequency was 3846 Hz which corresponds to a 260 μs rotor period. FSLG homonuclear decoupling was applied with an 81.7 kHz RF field, which corresponds to FSLG 2π-pulse widths which are 10 μs in duration. The $^{15}N/^{13}C$ dipolar evolution time preceding the $^{15}N/^{13}C$ π-pulse (denoted as t_1) was then stepped in increments of 20 μs, which corresponds to a complete FSLG cycle. 100 kHz SPINAL-64 heteronuclear decoupling was then applied during the second rotor period and signal acquisition. The ^{1}H-^{15}N DIPSHIFT spectra were recorded with recycle delays between 15-20 s, and between 48-272 scans were acquired for each of the 13 individual t_1 increments (Table S1). The ^{1}H-^{13}C DIPSHIFT spectra were obtained with a 15 s recycle delay, 8 scans per increment and 13 individual t_1 increments with t_1 incremented in steps of 20 μs.

Conventional solid-state NMR experiments were performed at Genentech Inc. using a Bruker Avance III HD spectrometer equipped with a standard bore 11.7 T magnet and 4 mm double resonance MAS probe. Samples were packed into 4 mm zirconia rotors, sealed with Kel-F drive tips. The MAS frequency was 8 kHz and the sample temperature was controlled at 293 K. Recycle delays were set to 1.5-7 s dependent on T_1, and CP contact times were 3 ms for ^{13}C and 5 ms for ^{15}N experiments, with a 70-100% ^{1}H RF field ramp. SPINAL-64 ^{1}H decoupling was applied at a 90 kHz field strength for all conventional experiments, and TOSS was applied to suppress spinning sidebands.

Numerical simulations of the dipole-doubled DIPSHIFT and PRESTO-II ^{1}H-^{15}N solid-state NMR experiments were performed with the SIMPSON *v*4.1.1 program[110-112] running on personal computers. Plane-wave DFT calculations were used to determine the relative orientation of the ^{1}H chemical shift (CS) tensor and the ^{1}H-^{15}N dipole-vector. The Euler angles describing the

relative orientation of the ^{1}H CS tensor and ^{1}H-^{15}N dipole-vector were included in SUNOSIB simulations of the PRESTO-II dipolar oscillations for **A3**

Plane-wave DFT calculations. All calculations were performed using plane-wave pseudopotential periodic DFT as implemented in CASTEP code.[113] All calculations used the Perdew–Burke–Ernzerhof generalized gradient approximation (PBE-GGA) functional[114] with ultra-soft pseudopotentials generated on-the-fly.[115] The Grimme DFT-D2 dispersion correction scheme used in all calculations.[116] The wavefunctions were expanded using a plane wave basis set with a kinetic energy cut-off of 630 eV that produces converged results for both the geometry optimization and the calculation of NMR parameters. NMR shielding values were calculated using the GIPAW method[117] as implemented in the CASTEP code. The integrals were calculated over the Brillouin zone were performed using a Monkhorst–Pack grid with a *k*-point spacing of 0.07 Å^{-1}. Heavy atom positions and unit cell parameters were taken from the single-crystal X-ray diffraction structures and all H atom positions were optimized prior to calculation of NMR properties. Calculated ^{15}N magnetic isotropic magnetic shielding values (σ_{iso}) were converted to ^{15}N isotropic chemical shift values (δ_{iso}) by making a plot of experimental δ_{iso} as function of calculated σ_{iso} for **A1**-**A3** and histidine•HCl•H_2O (Figure S12). Linear regression analysis yielded the calibration equation $\delta_{iso,\,calc} = -1.0084 \times [\sigma_{iso,\,calc}] - 160.0$ that was used to convert calculated magnetic shielding to calculated chemical shift values. This calibration equation is very similar to the equation $\delta_{iso,\,calc} = -1.017 \times [\sigma_{iso,\,calc}] - 156.0$ previously determined by Beran and co-workers for GIPAW-PBE calculations of nitrogen chemical shifts.[118] Note that a conversion factor of –341 ppm was used to convert the Beran equation from the NH_4Cl ^{15}N chemical shift scale to the IUPAC nitromethane ^{15}N chemical shift scale.

ELECTRONIC SUPPLEMENTARY INFORMATION

Additional solid-state NMR spectra, sample preparation, single crystal X-ray diffraction structures of **A1-A3**, data analysis and details on spectral processing.

ACKNOWLEDGMENTS

This material is based upon work supported by the National Science Foundation under Grant No. 1709972 to AJR. We thank Genentech, Inc. and its Innovation Fund, for providing financial support for this work. AJR also thanks Iowa State University and the Ames Laboratory (Royalty Account) for additional support. The Ames Laboratory is operated for the U.S. DOE by Iowa State University under contract no. DE-AC02-07CH11358. We are grateful to Dr. Marek Pruski (DOE Ames Laboratory) and his research group for providing access to and assistance with the DNP solid-state NMR spectrometer. We thank Dr. Frédéric Perras for advice and discussions about PRESTO solid-state NMR experiments.

REFERENCES:

[1] Almarsson, O.; Zaworotko, M. J. Crystal Engineering of the Composition of Pharmaceutical Phases. Do Pharmaceutical Co-Crystals Represent a New Path to Improved Medicines? *Chem. Commun.* **2004**, 1889-1896.
[2] Jones, W.; Motherwell, S.; Trask, A. V. Pharmaceutical Cocrystals: An Emerging Approach to Physical Property Enhancement. *MRS Bull.* **2006**, *31*, 875-879.
[3] Childs, S. L.; Stahly, G. P.; Park, A. The Salt-Cocrystal Continuum: The Influence of Crystal Structure on Ionization State. *Mol. Pharm.* **2007**, *4*, 323-338.
[4] Stahly, G. P. Diversity in Single- and Multiple-Component Crystals. The Search for and Prevalence of Polymorphs and Cocrystals. *Crystal Growth & Design* **2007**, *7*, 1007-1026.
[5] Schultheiss, N.; Newman, A. Pharmaceutical Cocrystals and Their Physicochemical Properties. *Crystal Growth & Design* **2009**, *9*, 2950-2967.
[6] Friscic, T.; Jones, W. Benefits of Cocrystallisation in Pharmaceutical Materials Science: An Update. *J. Pharm. Pharmacol.* **2010**, *62*, 1547-1559.
[7] Douroumis, D.; Nokhodchi, A. Preface: Engineering of Pharmaceutical Cocrystals, Salts and Polymorphs: Advances and Challenges. *Advanced Drug Delivery Reviews* **2017**, *117*, 1-2.
[8] Rajput, L.; Banik, M.; Yarava, J. R.; Joseph, S.; Pandey, M. K.; Nishiyama, Y.; Desiraju, G. R. Exploring the Salt-Cocrystal Continuum with Solid-State NMR Using Natural-Abundance Samples: Implications for Crystal Engineering. *IUCrJ* **2017**, *4*.
[9] Steiner, T.; Majerz, I.; Wilson, C. C. First O− H− N Hydrogen Bond with a Centered Proton Obtained by Thermally Induced Proton Migration. *Angew. Chem., Int. Ed.* **2001**, *40*, 2651-2654.
[10] Parkin, A.; Harte, S. M.; Goeta, A. E.; Wilson, C. C. Imaging Proton Migration from X-Rays and Neutrons. *New J. Chem.* **2004**, *28*, 718-721.
[11] Hasa, D.; Jones, W. Screening for New Pharmaceutical Solid Forms Using Mechanochemistry: A Practical Guide. *Advanced Drug Delivery Reviews* **2017**, *117*, 147-161.
[12] Lusi, M.; Barbour, L. J. Determining Hydrogen Atom Positions for Hydrogen Bonded Interactions: A Distance-Dependent Neutron-Normalized Method. *Crystal Growth & Design* **2011**, *11*, 5515-5521.
[13] Deringer, V. L.; Hoepfner, V.; Dronskowski, R. Accurate Hydrogen Positions in Organic Crystals: Assessing a Quantum-Chemical Aide. *Crystal Growth & Design* **2012**, *12*, 1014-1021.
[14] Stevens, J. S.; Byard, S. J.; Schroeder, S. L. Characterization of Proton Transfer in Co-Crystals by X-Ray Photoelectron Spectroscopy (XPS). *Crystal Growth & Design* **2010**, *10*, 1435-1442.
[15] Stevens, J. S.; Byard, S. J.; Muryn, C. A.; Schroeder, S. L. M. Identification of Protonation State by XPS, Solid-State Nmr, and Dft: Characterization of the Nature of a New Theophylline Complex by Experimental and Computational Methods. *J. Phys. Chem. B* **2010**, *114*, 13961-13969.
[16] Stevens, J. S.; Byard, S. J.; Schroeder, S. L. M. Salt or Co-Crystal? Determination of Protonation State by X-Ray Photoelectron Spectroscopy (Xps). *J. Pharm. Sci.* **2010**, *99*, 4453-4457.
[17] Pindelska, E.; Sokal, A.; Kolodziejski, W. Pharmaceutical Cocrystals, Salts and Polymorphs: Advanced Characterization Techniques. *Advanced Drug Delivery Reviews* **2017**, *117*, 111-146.

[18] Berendt, R. T.; Sperger, D. M.; Isbester, P. K.; Munson, E. J. Solid-State NMR Spectroscopy in Pharmaceutical Research and Analysis. *Trac-Trends in Analytical Chemistry* **2006**, *25*, 977-984.
[19] Harris, R. K. Nmr Studies of Organic Polymorphs & Solvates. *Analyst* **2006**, *131*, 351-373.
[20] Vogt, F. G.; Clawson, J. S.; Strohmeier, M.; Edwards, A. J.; Pham, T. N.; Watson, S. A. Solid-State NMR Analysis of Organic Cocrystals and Complexes. *Crystal Growth & Design* **2009**, *9*, 921-937.
[21] Vogt, F. G. Evolution of Solid-State NMR in Pharmaceutical Analysis. *Future Medicinal Chemistry* **2010**, *2*, 915-921.
[22] Li, Z. J.; Abramov, Y.; Bordner, J.; Leonard, J.; Medek, A.; Trask, A. V. Solid-State Acid−Base Interactions in Complexes of Heterocyclic Bases with Dicarboxylic Acids: Crystallography, Hydrogen Bond Analysis, and 15N NMR Spectroscopy. *J. Am. Chem. Soc.* **2006**, *128*, 8199-8210.
[23] Bouchmella, K.; Dutremez, S. G.; Alonso, B.; Mauri, F.; Gervais, C. 1H, 13C, and 15N Solid-State NMR Studies of Imidazole- and Morpholine-Based Model Compounds Possessing Halogen and Hydrogen Bonding Capabilities. *Crystal Growth & Design* **2008**, *8*, 3941-3950.
[24] Song, X.-j.; Rienstra, C. M.; McDermott, A. E. N—H Bond Stretching in Histidine Complexes: A Solid-State NMR Study. *Magn. Reson. Chem.* **2001**, *39*, S30-S36.
[25] Tatton, A. S.; Pham, T. N.; Vogt, F. G.; Iuga, D.; Edwards, A. J.; Brown, S. P. Probing Intermolecular Interactions and Nitrogen Protonation in Pharmaceuticals by Novel N-15-Edited and 2D N-14-H-1 Solid-State NMR. *Crystengcomm* **2012**, *14*, 2654-2659.
[26] Gaglioti, K.; Chierotti, M. R.; Grifasi, F.; Gobetto, R.; Griesser, U. J.; Hasa, D.; Voinovich, D. Improvement of the Water Solubility of Tolfenamic Acid by New Multiple-Component Crystals Produced by Mechanochemical Methods. *Crystengcomm* **2014**, *16*, 8252-8262.
[27] Song, Y.; Yang, X.; Chen, X.; Nie, H.; Byrn, S.; Lubach, J. W. Investigation of Drug–Excipient Interactions in Lapatinib Amorphous Solid Dispersions Using Solid-State NMR Spectroscopy. *Mol. Pharm.* **2015**, *12*, 857-866.
[28] Mistry, P.; Mohapatra, S.; Gopinath, T.; Vogt, F. G.; Suryanarayanan, R. Role of the Strength of Drug–Polymer Interactions on the Molecular Mobility and Crystallization Inhibition in Ketoconazole Solid Dispersions. *Mol. Pharm.* **2015**, *12*, 3339-3350.
[29] Song, Y.; Zemlyanov, D.; Chen, X.; Nie, H.; Su, Z.; Fang, K.; Yang, X.; Smith, D.; Byrn, S.; Lubach, J. W. Acid–Base Interactions of Polystyrene Sulfonic Acid in Amorphous Solid Dispersions Using a Combined UV/FTIR/XPS/SSNMR Study. *Mol. Pharm.* **2016**, *13*, 483-492.
[30] Tatton, A. S.; Pham, T. N.; Vogt, F. G.; Iuga, D.; Edwards, A. J.; Brown, S. P. Probing Hydrogen Bonding in Cocrystals and Amorphous Dispersions Using N-14-H-1 HMQC Solid-State NMR. *Mol. Pharm.* **2013**, *10*, 999-1007.
[31] Lesage, A.; Steuernagel, S.; Emsley, L. Carbon-13 Spectral Editing in Solid-State NMR Using Heteronuclear Scalar Couplings. *J. Am. Chem. Soc.* **1998**, *120*, 7095-7100.
[32] Khan, M.; Enkelmann, V.; Brunklaus, G. Heterosynthon Mediated Tailored Synthesis of Pharmaceutical Complexes: A Solid-State Nmr Approach. *Crystengcomm* **2011**, *13*, 3213-3223.
[33] Luedeker, D.; Gossmann, R.; Langer, K.; Brunklaus, G. Crystal Engineering of Pharmaceutical Co-Crystals:"NMR Crystallography" of Niclosamide Co-Crystals. *Cryst. Growth Des* **2016**, *16*, 3087-3100.
[34] Vigilante, N. J.; Mehta, M. A. A 13C Solid-State NMR Investigation of Four Cocrystals of Caffeine and Theophylline. *Acta Crystallographica Section C* **2017**, *73*, 234-243.

[35] Lüdeker, D.; Brunklaus, G. NMR Crystallography of Ezetimibe Co-Crystals. *Solid State Nuclear Magnetic Resonance* **2015**, *65*, 29-40.
[36] Zhao, X.; Sudmeier, J. L.; Bachovchin, W. W.; Levitt, M. H. Measurement of NH Bond Lengths by Fast Magic-Angle Spinning Solid-State NMR Spectroscopy: A New Method for the Quantification of Hydrogen Bonds. *J. Am. Chem. Soc.* **2001**, *123*, 11097-11098.
[37] Goward, G. R.; Schnell, I.; Brown, S. P.; Spiess, H. W.; Kim, H.-D.; Ishida, H. Investigation of an N···H Hydrogen Bond in a Solid Benzoxazine Dimer by 1H–15N NMR Correlation Techniques under Fast Magic-Angle Spinning. *Magn. Reson. Chem.* **2001**, *39*, S5-S17.
[38] Zhao, L.; Li, W.; Plog, A.; Xu, Y.; Buntkowsky, G.; Gutmann, T.; Zhang, K. Multi-Responsive Cellulose Nanocrystal-Rhodamine Conjugates: An Advanced Structure Study by Solid-State Dynamic Nuclear Polarization (DNP) NMR. *Phys. Chem. Chem. Phys.* **2014**, *16*, 26322-26329.
[39] Zhao, L.; Smolarkiewicz, I.; Limbach, H.-H.; Breitzke, H.; Pogorzelec-Glaser, K.; Pankiewicz, R.; Tritt-Goc, J.; Gutmann, T.; Buntkowsky, G. Imidazole-Doped Cellulose as Membrane for Fuel Cells: Structural and Dynamic Insights from Solid-State NMR. *J. Phys. Chem. C* **2016**, *120*, 19574-19585.
[40] Veinberg, S. L.; Johnston, K. E.; Jaroszewicz, M. J.; Kispal, B. M.; Mireault, C. R.; Kobayashi, T.; Pruski, M.; Schurko, R. W. Natural Abundance 14N and 15N Solid-State NMR of Pharmaceuticals and Their Polymorphs. *Phys. Chem. Chem. Phys.* **2016**, *18*, 17713-17730.
[41] Schnell, I.; Saalwächter, K. 15N−H Bond Length Determination in Natural Abundance by Inverse Detection in Fast-MAS Solid-State NMR Spectroscopy. *J. Am. Chem. Soc.* **2002**, *124*, 10938-10939.
[42] Li, S.; Hong, M. Protonation, Tautomerization, and Rotameric Structure of Histidine: A Comprehensive Study by Magic-Angle-Spinning Solid-State Nmr. *Journal of the American Chemical Society* **2011**, *133*, 1534-1544.
[43] Shenderovich, I. G.; Lesnichin, S. B.; Tu, C.; Silverman, D. N.; Tolstoy, P. M.; Denisov, G. S.; Limbach, H.-H. NMR Studies of Active-Site Properties of Human Carbonic Anhydrase Ii by Using 15N-Labeled 4-Methylimidazole as a Local Probe and Histidine Hydrogen-Bond Correlations. *Chem. Eur. J.* **2015**, *21*, 2915-2929.
[44] Becerra, L. R.; Gerfen, G. J.; Temkin, R. J.; Singel, D. J.; Griffin, R. G. Dynamic Nuclear-Polarization with a Cyclotron-Resonance Maser at 5-T. *Phys. Rev. Lett.* **1993**, *71*, 3561-3564.
[45] Hall, D. A.; Maus, D. C.; Gerfen, G. J.; Inati, S. J.; Becerra, L. R.; Dahlquist, F. W.; Griffin, R. G. Polarization-Enhanced Nmr Spectroscopy of Biomolecules in Frozen Solution. *Science* **1997**, *276*, 930-932.
[46] Maly, T.; Debelouchina, G. T.; Bajaj, V. S.; Hu, K. N.; Joo, C. G.; Mak-Jurkauskas, M. L.; Sirigiri, J. R.; van der Wel, P. C. A.; Herzfeld, J.; Temkin, R. J.; Griffin, R. G. Dynamic Nuclear Polarization at High Magnetic Fields. *J. Chem. Phys.* **2008**, *128*, 052211.
[47] Ni, Q. Z.; Daviso, E.; Can, T. V.; Markhasin, E.; Jawla, S. K.; Swager, T. M.; Temkin, R. J.; Herzfeld, J.; Griffin, R. G. High Frequency Dynamic Nuclear Polarization. *Acc. Chem. Res.* **2013**, *48*, 1933–1941.
[48] van der Wel, P. C. A.; Hu, K. N.; Lewandowski, J.; Griffin, R. G. Dynamic Nuclear Polarization of Amyloidogenic Peptide Nanocrystals: GNNQQNY, a Core Segment of the Yeast Prion Protein Sup35p. *J. Am. Chem. Soc.* **2006**, *128*, 10840-10846.
[49] Rossini, A. J.; Zagdoun, A.; Hegner, F. S.; Schwarzwälder, M.; Gajan, D.; Copéret, C.; Lesage, A.; Emsley, L. Dynamic Nuclear Polarization NMR Spectroscopy of Microcrystalline Solids. *J. Am. Chem. Soc.* **2012**, *134*, 16899−16908.

[50] Rossini, A. J.; Widdifield, C. M.; Zagdoun, A.; Lelli, M.; Schwarzwälder, M.; Copéret, C.; Lesage, A.; Emsley, L. Dynamic Nuclear Polarization Enhanced NMR Spectroscopy for Pharmaceutical Formulations. *J. Am. Chem. Soc.* **2014**, *136*, 2324-2334.
[51] Ji, X.; Bornet, A.; Vuichoud, B.; Milani, J.; Gajan, D.; Rossini, A. J.; Emsley, L.; Bodenhausen, G.; Jannin, S. Transportable Hyperpolarized Metabolites. *Nat. Commun.* **2017**, *8*, 13975.
[52] Zhao, L.; Pinon, A. C.; Emsley, L.; Rossini, A. J. DNP-Enhanced Solid-State NMR Spectroscopy of Active Pharmaceutical Ingredients. *Magn. Reson. Chem.* **2018**, *In Press, DOI: 10.1002/mrc.4688*
[53] Lesage, A.; Lelli, M.; Gajan, D.; Caporini, M. A.; Vitzthum, V.; Mieville, P.; Alauzun, J.; Roussey, A.; Thieuleux, C.; Mehdi, A.; Bodenhausen, G.; Copéret, C.; Emsley, L. Surface Enhanced NMR Spectroscopy by Dynamic Nuclear Polarization. *J. Am. Chem. Soc.* **2010**, *132*, 15459-15461.
[54] Zagdoun, A.; Rossini, A. J.; Gajan, D.; Bourdolle, A.; Ouari, O.; Rosay, M.; Maas, W. E.; Tordo, P.; Lelli, M.; Emsley, L.; Lesage, A.; Copéret, C. Nonaqueous Solvents for DNP Spectroscopy. *Chem. Commun.* **2012**, *48*, 654-656.
[55] Takahashi, H.; Lee, D.; Dubois, L.; Bardet, M.; Hediger, S.; De Paëpe, G. Rapid Natural-Abundance 2D 13C–13C Correlation Spectroscopy Using Dynamic Nuclear Polarization Enhanced Solid-State Nmr and Matrix Free Sample Preparation. *Angew. Chem.- Int. Ed.* **2012**, *124*, 11936 –11939.
[56] Takahashi, H.; Hediger, S.; De Paëpe, G. Matrix-Free Dynamic Nuclear Polarization Enables Solid-State Nmr 13 C–13 C Correlation Spectroscopy of Proteins at Natural Isotopic Abundance. *Chemical Communications* **2013**, *49*, 9479-9481.
[57] Mollica, G.; Dekhil, M.; Ziarelli, F.; Thureau, P.; Viel, S. Quantitative Structural Constraints for Organic Powders at Natural Isotopic Abundance Using Dynamic Nuclear Polarization Solid-State Nmr Spectroscopy. *Angew. Chem. Int. Ed.* **2015**, *54*, 6028-6031.
[58] Leclaire, J.; Poisson, G.; Ziarelli, F.; Pepe, G.; Fotiadu, F.; Paruzzo, F. M.; Rossini, A. J.; Dumez, J.-N.; Elena-Herrmann, B.; Emsley, L. Structure Elucidation of a Complex CO2-Based Organic Framework Material by Nmr Crystallography. *Chem. Sci.* **2016**, *7*, 4379-4390.
[59] Märker, K.; Pingret, M.; Mouesca, J.-M.; Gasparutto, D.; Hediger, S.; De Paëpe, G. A New Tool for NMR Crystallography: Complete 13C/15N Assignment of Organic Molecules at Natural Isotopic Abundance Using Dnp-Enhanced Solid-State Nmr. *J. Am. Chem. Soc.* **2015**, *137*, 13796-13799.
[60] Rossini, A. J.; Schlagnitweit, J.; Lesage, A.; Emsley, L. High-Resolution NMR of Hydrogen in Organic Solids by DNP Enhanced Natural Abundance Deuterium Spectroscopy. *J. Magn. Reson.* **2015**, *259*, 192-198.
[61] Rossini, A. J.; Emsley, L.; O'Dell, L. A. Dynamic Nuclear Polarisation Enhanced 14N Overtone MAS NMR Spectroscopy. *Phys. Chem. Chem. Phys.* **2014**, *16*, 12890-12899.
[62] Rossini, A. J.; Zagdoun, A.; Lelli, M.; Canivet, J.; Aguado, S.; Ouari, O.; Tordo, P.; Rosay, M.; Maas, W. E.; Copéret, C.; Farrusseng, D.; Emsley, L.; Lesage, A. Dynamic Nuclear Polarization Enhanced Solid-State NMR Spectroscopy of Functionalized Metal-Organic Frameworks. *Angew. Chem.- Int. Ed.* **2012**, *51*, 123-127.
[63] Blanc, F.; Sperrin, L.; Jefferson, D. A.; Pawsey, S.; Rosay, M.; Grey, C. P. Dynamic Nuclear Polarization Enhanced Natural Abundance 17O Spectroscopy. *J. Am. Chem. Soc.* **2013**, *135*, 2975-2978.

[64] Hirsh, D. A.; Rossini, A. J.; Emsley, L.; Schurko, R. W. 35Cl Dynamic Nuclear Polarization Solid-State NMR of Active Pharmaceutical Ingredients. *Phys. Chem. Chem. Phys.* **2016**, *18*, 25893-25904.
[65] Lee, D.; Leroy, C.; Crevant, C.; Bonhomme-Coury, L.; Babonneau, F.; Laurencin, D.; Bonhomme, C.; De Paëpe, G. Interfacial Ca2+ Environments in Nanocrystalline Apatites Revealed by Dynamic Nuclear Polarization Enhanced 43Ca NMR Spectroscopy. *Nat. Commun.* **2017**, *8*, 14104.
[66] Blanc, F.; Sperrin, L.; Lee, D.; Dervisoglu, R.; Yamazaki, Y.; Haile, S. M.; De Paepe, G.; Grey, C. P. Dynamic Nuclear Polarization NMR of Low-Gamma Nuclei: Structural Insights into Hydrated Yttrium-Doped BaZrO3. *J. Phys. Chem. Lett.* **2014**, *5*, 2431-2436.
[67] Huang, K.-S.; Britton, D.; late Margaret C. Etter, t.; Byrn, S. R. A Novel Class of Phenol-Pyridine Co-Crystals for Second Harmonic Generation. *J. Mater. Chem.* **1997**, *7*, 713-720.
[68] Childs, S. L.; Stahly, G. P.; Park, A. The Salt−Cocrystal Continuum: The Influence of Crystal Structure on Ionization State. *Molecular Pharmaceutics* **2007**, *4*, 323-338.
[69] Wilson, C. C.; Goeta, A. E. Towards Designing Proton-Transfer Systems—Direct Imaging of Proton Disorder in a Hydrogen-Bonded Carboxylic Acid Dimer by Variable-Temperature X-Ray Diffraction. *Angewandte Chemie International Edition* **2004**, *43*, 2095-2099.
[70] Bhogala, B. R.; Basavoju, S.; Nangia, A. Tape and Layer Structures in Cocrystals of Some Di-and Tricarboxylic Acids with 4, 4'-Bipyridines and Isonicotinamide. From Binary to Ternary Cocrystals. *Crystengcomm* **2005**, *7*, 551-562.
[71] Lubben, J.; Volkmann, C.; Grabowsky, S.; Edwards, A.; Morgenroth, W.; Fabbiani, F. P. A.; Sheldrick, G. M.; Dittrich, B. On the Temperature Dependence of H-Uiso in the Riding Hydrogen Model. *Acta Crystallographica Section A* **2014**, *70*, 309-316.
[72] Pinon, A. C.; Rossini, A. J.; Widdifield, C. M.; Gajan, D.; Emsley, L. Polymorphs of Theophylline Characterized by DNP Enhanced Solid-State NMR. *Mol. Pharm.* **2015**, *12*, 4146-4153.
[73] Zagdoun, A.; Casano, G.; Ouari, O.; Schwarzwälder, M.; Rossini, A. J.; Aussenac, F.; M., Y.; G., J.; Copéret, C.; Lesage, A.; Tordo, P.; Emsley, L. Large Molecular Weight Nitroxide Biradicals Providing Efficient Dynamic Nuclear Polarization at Temperatures up to 200 K. *J. Am. Chem. Soc.* **2013**, *135*, 12790-12797.
[74] Pines, A.; Gibby, M. G.; Waugh, J. S. Proton-Enhanced NMR of Dilute Spins in Solids. *J. Chem. Phys.* **1973**, *59*, 569-590.
[75] Schaefer, J.; Stejskal, E. O. C-13 Nuclear Magnetic-Resonance of Polymers Spinning at Magic Angle. *J. Am. Chem. Soc.* **1976**, *98*, 1031-1032.
[76] Ni, Q. Z.; Yang, F.; Can, T. V.; Sergeyev, I. V.; D'Addio, S. M.; Jawla, S. K.; Li, Y.; Lipert, M. P.; Xu, W.; Williamson, R. T.; Leone, A.; Griffin, R. G.; Su, Y. In-Situ Characterization of Pharmaceutical Formulations by Dynamic Nuclear Polarization Enhanced MAS NMR. *Journal of Physical Chemistry B* **2017**, *121*, 8132–8141.
[77] Dixon, W. T.; Schaefer, J.; Sefcik, M. D.; Stejskal, E. O.; McKay, R. A. Total Suppression of Sidebands in CPMAS C-13 NMR. *J. Magn. Reson.* **1982**, *49*, 341-345.
[78] Dixon, W. T. Spinning - Sideband - Free and Spinning - Sideband - Only NMR Spectra in Spinning Samples. *J. Chem. Phys.* **1982**, *77*, 1800-1809.
[79] Solum, M. S.; Altmann, K. L.; Strohmeier, M.; Berges, D. A.; Zhang, Y.; Facelli, J. C.; Pugmire, R. J.; Grant, D. M. 15N Chemical Shift Principal Values in Nitrogen Heterocycles. *Journal of the American Chemical Society* **1997**, *119*, 9804-9809.

[80] Elena, B.; de Paëpe, G.; Emsley, L. Direct Spectral Optimisation of Proton–Proton Homonuclear Dipolar Decoupling in Solid-State NMR. *Chemical Physics Letters* **2004**, *398*, 532-538.
[81] Salager, E.; Stein, R. S.; Pickard, C. J.; Elena, B.; Emsley, L. Powder NMR Crystallography of Thymol. *Phys. Chem. Chem. Phys.* **2009**, *11*, 2610-2621.
[82] Salager, E.; Day, G. M.; Stein, R. S.; Pickard, C. J.; Elena, B.; Emsley, L. Powder Crystallography by Combined Crystal Structure Prediction and High-Resolution 1H Solid-State NMR Spectroscopy. *Journal of the American Chemical Society* **2010**, *132*, 2564-2566.
[83] Baias, M.; Widdifield, C. M.; Dumez, J.-N.; Thompson, H. P. G.; Cooper, T. G.; Salager, E.; Bassil, S.; Stein, R. S.; Lesage, A.; Day, G. M.; Emsley, L. Powder Crystallography of Pharmaceutical Materials by Combined Crystal Structure Prediction and Solid-State 1H NMR Spectroscopy. *Physical Chemistry Chemical Physics* **2013**, *15*, 8069-8080.
[84] Santos, S. M.; Rocha, J.; Mafra, L. Nmr Crystallography: Toward Chemical Shift-Driven Crystal Structure Determination of the B-Lactam Antibiotic Amoxicillin Trihydrate. *Crystal Growth & Design* **2013**, *13*, 2390-2395.
[85] Ashbrook, S. E.; McKay, D. Combining Solid-State NMR Spectroscopy with First-Principles Calculations - a Guide to Nmr Crystallography. *Chemical Communications* **2016**, *52*, 7186-7204.
[86] Widdifield, C. M.; Robson, H.; Hodgkinson, P. Furosemide's One Little Hydrogen Atom: NMR Crystallography Structure Verification of Powdered Molecular Organics. *Chem. Commun.* **2016**, *52*, 6685-6688.
[87] Hofstetter, A.; Emsley, L. Positional Variance in NMR Crystallography. *J. Am. Chem. Soc.* **2017**, *139*, 2573-2576.
[88] Ladizhansky, V.; Vega, S. A Method for Measuring Heteronuclear (1H−13C) Distances in High Speed MAS NMR. *Journal of the American Chemical Society* **2000**, *122*, 3465-3472.
[89] Terao, T.; Miura, H.; Saika, A. High - Resolution J - Resolved NMR Spectra of Dilute Spins in Solids. *J. Chem. Phys.* **1981**, *75*, 1573-1574.
[90] Trébosc, J.; Amoureux, J. P.; Delevoye, L.; Wiench, J. W.; Pruski, M. Frequency-Selective Measurement of Heteronuclear Scalar Couplings in Solid-State NMR. *Solid State Sciences* **2004**, *6*, 1089-1095.
[91] Fitzkee, N. C.; Bax, A. Facile Measurement of (1)H-(15)N Residual Dipolar Couplings in Larger Perdeuterated Proteins. *Journal of biomolecular NMR* **2010**, *48*, 65-70.
[92] Althaus, S. M.; Mao, K.; Stringer, J. A.; Kobayashi, T.; Pruski, M. Indirectly Detected Heteronuclear Correlation Solid-State NMR Spectroscopy of Naturally Abundant 15N Nuclei. *Solid State Nucl. Magn. Reson.* **2014**, *57-58*, 17-21.
[93] Blanc, F.; Coperet, C.; Lesage, A.; Emsley, L. High Resolution Solid State NMR Spectroscopy in Surface Organometallic Chemistry: Access to Molecular Understanding of Active Sites of Well-Defined Heterogeneous Catalysts. *Chemical Society Reviews* **2008**, *37*, 518-526.
[94] Lesage, A.; Emsley, L.; Chabanas, M.; Copéret, C.; Basset, J.-M. Observation of a H-Agostic Bond in a Highly Active Rhenium–Alkylidene Olefin Metathesis Heterogeneous Catalyst by Two-Dimensional Solid-State NMR Spectroscopy. *Angew. Chem., Int. Ed.* **2002**, *41*, 4535-4538.
[95] Salager, E.; Stein, R. S.; Steuernagel, S.; Lesage, A.; Elena, B.; Emsley, L. Enhanced Sensitivity in High-Resolution H-1 Solid-State NMR Spectroscopy with Dumbo Dipolar Decoupling under Ultra-Fast Mas. *Chem. Phys. Lett.* **2009**, *469*, 336-341.

[96] Hong, M.; Gross, J. D.; Rienstra, C. M.; Griffin, R. G.; Kumashiro, K. K.; Schmidt-Rohr, K. Coupling Amplification in 2D MAS NMR and Its Application to Torsion Angle Determination in Peptides. *J. Magn. Reson.* **1997**, *129*, 85-92.
[97] Zhao, X.; Hoffbauer, W.; auf der Günne, J. S.; Levitt, M. H. Heteronuclear Polarization Transfer by Symmetry-Based Recoupling Sequences in Solid-State NMR. *Solid state nuclear magnetic resonance* **2004**, *26*, 57-64.
[98] Fuess, H.; Hohlwein, D.; Mason, S. Neutron Diffraction Study of L-Histidine Hydrochloride Monohydrate. *Acta Crystallographica Section B: Structural Crystallography and Crystal Chemistry* **1977**, *33*, 654-659.
[99] Redfield, A. G. Nuclear Magnetic Resonance Saturation and Rotary Saturation in Solids. *Phys. Rev.* **1955**, *98*, 1787-1809.
[100] Lee, M.; Goldburg, W. I. Nuclear-Magnetic-Resonance Line Narrowing by a Rotating RF Field. *Physical Review* **1965**, *140*, A1261.
[101] Bielecki, A.; Kolbert, A.; De Groot, H.; Griffin, R.; Levitt, M. Frequency-Switched Lee-Goldburg Sequences in Solids. *Adv. Magn. Reson* **1990**, *14*.
[102] Perras, F. A.; Kobayashi, T.; Pruski, M. Natural Abundance 17O DNP Two-Dimensional and Surface-Enhanced NMR Spectroscopy. *J. Am. Chem. Soc.* **2015**, *137*, 8336–8339.
[103] Horiuchi, S.; Tokunaga, Y.; Giovannetti, G.; Picozzi, S.; Itoh, H.; Shimano, R.; Kumai, R.; Tokura, Y. Above-Room-Temperature Ferroelectricity in a Single-Component Molecular Crystal. *Nature* **2010**, *463*, 789-792.
[104] Rosay, M.; Tometich, L.; Pawsey, S.; Bader, R.; Schauwecker, R.; Blank, M.; Borchard, P. M.; Cauffman, S. R.; Felch, K. L.; Weber, R. T.; Temkin, R. J.; Griffin, R. G.; Maas, W. E. Solid-State Dynamic Nuclear Polarization at 263 GHz: Spectrometer Design and Experimental Results. *Phys. Chem. Chem. Phys.* **2010**, *12*, 5850-5860.
[105] Harris, R. K.; Becker, E. D.; De Menezes, S. M. C.; Goodfellow, R.; Granger, P. NMR Nomenclature. Nuclear Spin Properties and Conventions for Chemical Shifts - (IUPAC Recommendations 2001). *Pure Appl. Chem.* **2001**, *73*, 1795-1818.
[106] Stejskal, E. O.; Schaefer, J.; Waugh, J. S. Magic-Angle Spinning and Polarization Transfer in Proton-Enhanced Nmr. *J. Magn. Reson.* **1977**, *28*, 105-112.
[107] Peersen, O.; Wu, X.; Kustanovich, I.; Smith, S. Variable-Amplitude Cross-Polarization MAS NMR. *J. Magn. Reson., Ser A* **1993**, *104*, 334-339.
[108] Fung, B. M.; Khitrin, A. K.; Ermolaev, K. An Improved Broadband Decoupling Sequence for Liquid Crystals and Solids. *J. Magn. Reson.* **2000**, *142*, 97-101.
[109] Roberts, J. E.; Vega, S.; Griffin, R. G. Two-Dimensional Heteronuclear Chemical Shift Correlation Spectroscopy in Rotating Solids. *J. Am. Chem. Soc.* **1984**, *106*, 2506-2512.
[110] Bak, M.; Rasmussen, J. T.; Nielsen, N. C. Simpson: A General Simulation Program for Solid-State NMR Spectroscopy. *J. Magn. Reson.* **2000**, *147*, 296-330.
[111] Tosner, Z.; Vosegaard, T.; Kehlet, C.; Khaneja, N.; Glaser, S. J.; Nielsen, N. C. Optimal Control in NMR Spectroscopy: Numerical Implementation in SIMPSON. *J. Magn. Reson.* **2009**, *197*, 120-134.
[112] Tosner, Z.; Andersen, R.; Stevenss, B.; Eden, M.; Nielsen, N. C.; Vosegaard, T. Computer-Intensive Simulation of Solid-State NMR Experiments Using SIMPSON. *J. Magn. Reson.* **2014**, *246*, 79-93.
[113] Clark, S. J.; Segall, M. D.; Pickard, C. J.; Hasnip, P. J.; Probert, M. I.; Refson, K.; Payne, M. C. First Principles Methods Using CASTEP. *Zeitschrift für Kristallographie-Crystalline Materials* **2005**, *220*, 567-570.

[114] Perdew, J. P.; Burke, K.; Ernzerhof, M. Generalized Gradient Approximation Made Simple. *Phys. Rev. Lett.* **1996**, *77*, 3865-3868.
[115] Yates, J. R.; Pickard, C. J.; Mauri, F. Calculation of NMR Chemical Shifts for Extended Systems Using Ultrasoft Pseudopotentials. *Physical Review B* **2007**, *76*, 024401.
[116] Grimme, S. Semiempirical Gga-Type Density Functional Constructed with a Long-Range Dispersion Correction. *J. Comput. Chem.* **2006**, *27*, 1787-1799.
[117] Pickard, C. J.; Mauri, F. All-Electron Magnetic Response with Pseudopotentials: NMR Chemical Shifts. *Phys. Rev. B* **2001**, *63*, 245101.
[118] Hartman, J. D.; Kudla, R. A.; Day, G. M.; Mueller, L. J.; Beran, G. J. O. Benchmark Fragment-Based H-1, C-13, N-15 and O-17 Chemical Shift Predictions in Molecular Crystals. *Phys. Chem. Chem. Phys.* **2016**, *18*, 21686-21709.

TOC Graphic and TOC Synopsis

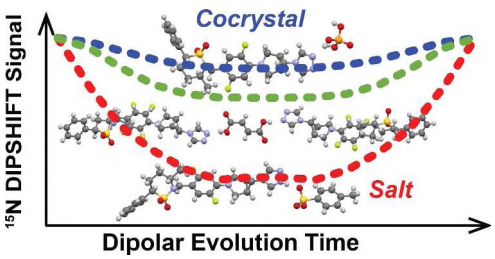

Dynamic nuclear polarization (DNP) accelerates natural isotopic abundance ^{15}N solid-state NMR experiments on multicomponent solids. DNP-enhanced double resonance ^{1}H-^{15}N NMR experiments allow ^{1}H-^{15}N dipolar coupling constants and H-N bond lengths to be accurately measured, providing an unambiguous assignment of nitrogen protonation state and definitive classification of the multicomponent solids as cocrystals or salts.